AD-A185 670 THE EFFECT OF LATITUDE ON THE DEVELOPMENT OF TROPICAL CYCLONES(U) AIR FORCE INST OF TECH WRIGHT-PATTERSON AFB OH J D PICKLE 1987 AFIT/CI/NR-87-95T 1/2

UNCLASSIFIED F/G 4/2 NL

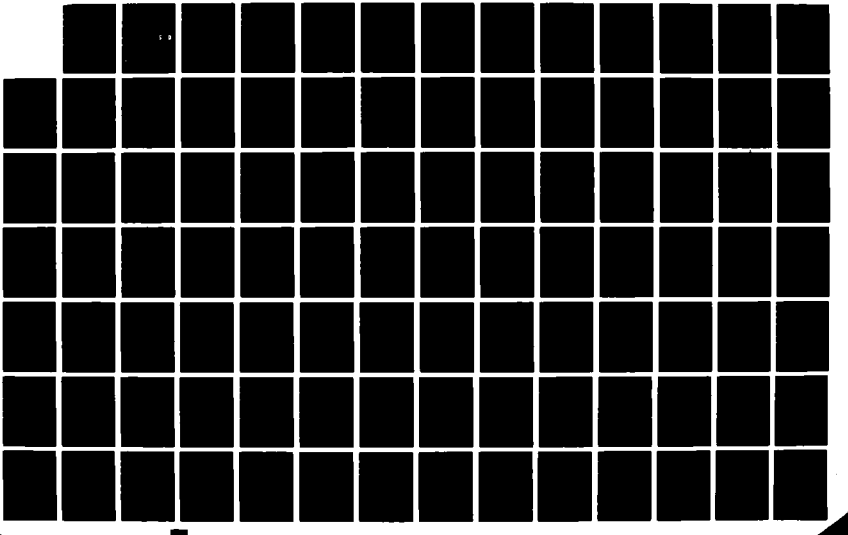

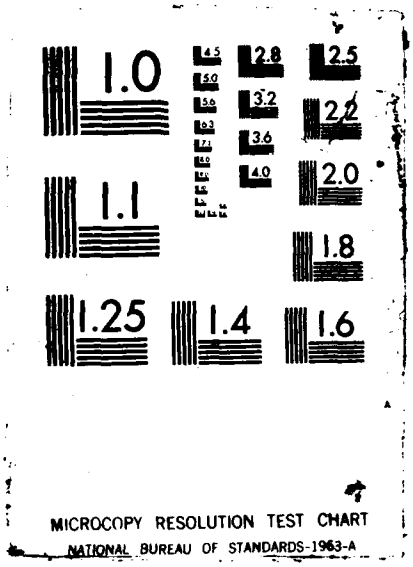
1.0
1.1
1.25
1.4
1.6
2.8
3.2
3.6
4.0
2.5
2.2
2.0
1.8
MICROCOPY RESOLUTION TEST CHART
NATIONAL BUREAU OF STANDARDS-1963-A

UNCLASSIFIED
SECURITY CLASSIFICATION OF THIS PAGE (When Data Entered)

REPORT DOCUMENTATION PAGE		READ INSTRUCTIONS BEFORE COMPLETING FORM
1. REPORT NUMBER AFIT/CI/NR 87-95T	2. GOVT ACCESSION NO. A185670	3. RECIPIENT'S CATALOG NUMBER
4. TITLE (and Subtitle) The Effect of Latitude on the Development of Tropical Cyclones		5. TYPE OF REPORT & PERIOD COVERED THESIS/DISSERTATION 6. PERFORMING ORG. REPORT NUMBER
7. AUTHOR(s) John David Pickle		8. CONTRACT OR GRANT NUMBER(s)
9. PERFORMING ORGANIZATION NAME AND ADDRESS AFIT STUDENT AT: North Carolina State University		10. PROGRAM ELEMENT, PROJECT, TASK AREA & WORK UNIT NUMBERS
11. CONTROLLING OFFICE NAME AND ADDRESS AFIT/NR WPAFB OH 45433-6583		12. REPORT DATE 1987 13. NUMBER OF PAGES 91
14. MONITORING AGENCY NAME & ADDRESS(if different from Controlling Office)		15. SECURITY CLASS. (of this report) UNCLASSIFIED 15a. DECLASSIFICATION/DOWNGRADING SCHEDULE

16. DISTRIBUTION STATEMENT (of this Report)

APPROVED FOR PUBLIC RELEASE; DISTRIBUTION UNLIMITED

DTIC ELECTE NOV 0 4 1987 S D

17. DISTRIBUTION STATEMENT (of the abstract entered in Block 20, if different from Report)

18. SUPPLEMENTARY NOTES

APPROVED FOR PUBLIC RELEASE: IAW AFR 190-1

LYNN E. WOLAVER 23 Oct 87
Dean for Research and
Professional Development
AFIT/NR

19. KEY WORDS (Continue on reverse side if necessary and identify by block number)

20. ABSTRACT (Continue on reverse side if necessary and identify by block number)

ATTACHED

DD FORM 1 JAN 73 1473 EDITION OF 1 NOV 65 IS OBSOLETE

SECURITY CLASSIFICATION OF THIS PAGE (When Data Entered)

AD-A185 670

DTIC FILE COPY

75

Abstract

The Effect of Latitude on the
Development of Tropical Cyclones
1Lt John David Pickle
United States Air Force
1987
91 pages
Master of Science
North Carolina State University

The three-layer balanced axisymmetric tropical cyclone model developed by Ooyama (1969) is generalized by relaxing the balance approximation and replacing the incompressible fluid layers with compressible fluid layers in isentropic coordinates. In numerical simulations the effects of latitude are non-linear; storms that intensify the fastest (at 10°N) do not intensify the most. When latitude is changed with other parameters held constant, storms between 20° and 30°N intensify the most. When the latitudinal change in sea surface temperature is considered, storms between 15° and 25°N intensify the most. The latter agrees with climatological trends observed in the western Pacific during 1980-1982. The effect of latitude is the dominant control of minimum surface pressure attained for lower latitudes (10°N); whereas northward, the effects of latitude and sea surface temperature are dominant. The size of storms is largely dependent upon latitude, where larger storms occur at more northerly latitudes.

Latitude influences the development of tropical cyclone growth by controlling the magnitude and radius of

maximum updraft. At lower latitudes, the zone of maximum updraft occurs closer to the center of the storm producing aerially smaller storms, and the rate of heating is greater than for more northerly storms. Both factors, combined with the increased heating efficiency caused by higher inertial stability values, allow the storm to intensify rapidly. However, because the rapid, more efficient heating quickly decreases the vertical instability, the period of intensification is shorter than at higher latitudes, producing only moderate to weak intensity storms.

95

The Effect of Latitude on the Development of Tropical Cyclones

by

John David Pickle

A thesis submitted to the Graduate Faculty of
North Carolina State University
in partial fulfillment of the
requirements for the Degree of
Master of Science

Department of Atmospheric Sciences

Raleigh

1987

Approved by:

Stephen Wright Vivian R Lamb

Mark DeMaria
Chairman of Advisory Committee

Abstract

PICKLE, JOHN D. The Effect of Latitude on the Development of Tropical Cyclones (Under the direction of Mark DeMaria).

The three-layer balanced axisymmetric tropical cyclone model developed by Ooyama (1969) is generalized by relaxing the balance approximation and replacing the incompressible fluid layers with compressible fluid layers in isentropic coordinates. The development of a cumulus parameterization scheme is simplified in isentropic coordinates. The primitive equations are solved using the spectral (Galerkin) method with Bessel function basis functions. In numerical situations, an increase in sea surface temperature or mid-level moisture increased the amount of moisture available for condensation per unit volume of ascending air. This resulted in a near-linear decrease in the minimum surface pressure attained, exponential increases in the maximum rate of intensification, and approximately no change in the size of storms (based on the radius of 30-knot winds) at maximum intensity.

The effects of latitude are non-linear; storms that intensify the fastest (at 10°N) do not intensify the most. When latitude is changed with other parameters held constant, storms between 20° and 30°N intensify the most. When the latitudinal change in sea surface temperature is considered, storms between 15° and 25°N intensify the most. The latter agrees with climatological trends observed in

the western Pacific during 1980-1982. The effect of latitude is the dominant control of minimum surface pressure attained for lower latitudes (10°N); whereas northward, the effects of latitude and sea surface temperature are dominant. The size of storms is largely dependent upon latitude, where larger storms occur at more northerly latitudes.

Latitude influences the development of tropical cyclone growth by controlling the magnitude and radius of maximum updraft. At lower latitudes, the zone of maximum updraft occurs closer to the center of the storm producing aerially smaller storms and the rate of heating is greater than for more northerly storms. Both factors, combined with the increased heating efficiency caused by higher inertial stability values, allow the storm to intensify rapidly. However, because the rapid, more efficient heating quickly decreases the vertical instability, the period of intensification is shorter than at higher latitudes, producing only moderate to weak intensity storms.

Table of Contents

Page

LIST OF FIGURES.....iii
LIST OF TABLES.....vi

1. INTRODUCTION.....1

2. MODEL DESCRIPTION.....6
   2.1 Governing Equations.....6
   2.2 Vertical Discretization.....8
   2.3 Parameterization of Physical Processes.....22
   2.4 Horizontal Discretization.....28
   2.5 Initial Conditions.....30

3. MODEL SIMULATIONS.....34
   3.1 Typical Model Simulation.....34
   3.2 Comparison of Cumulus Parameterization Schemes.....44
   3.3 Sensitivity Studies.....45
      3.3.1 Effect of Sea Surface Temperature.....48
      3.3.2 Effect of Mid-Level Moisture.....51
      3.3.3 Effect of Latitude.....54
      3.3.4 Effect of Sea Surface Temperature and Latitude.....56
      3.3.5 Effect of Seasonality.....63

4. COMPARISON WITH CLIMATOLOGY.....65
   4.1 Description of Data.....65
   4.2 Climatology of Tropical Cyclones Regardless of Developmental Stage.....70
   4.3 Climatology of Tropical Cyclones with Respect to Developmental Stage.....74

5. DISCUSSION AND SUMMARY.....80

6. LIST OF REFERENCES.....89

LIST OF FIGURES

1. Schematic representation of the three layers of the numerical simulation and the notation of the basic dependent variables.

2. Profiles of tangential winds in layers 0, 1, and 2 at t = 0, 48, and 96 hours.

3. Profiles of radial winds in layers 0, 1, and 2 at t = 0, 48, and 96 hours.

4. Minimum surface pressure, maximum tangential and radial winds with time.

5. Profiles of divergence in layers 0 and 2 at t = 0, 48, and 96 hours.

6. Profiles of the vertical stability parameter at t = 0, 48, and 96 hours.

7. Radii of maximum radial winds in layers 0, 1, and 2 with time.

8. Radii of maximum tangential winds in layers 0, 1, and 2 with time.

9. Radii of 30- and 50-knot tangential winds in layers 0 and 1 with time.

10. Comparison of results from the study numerical model and Ooyama's (1969) numerical model.

11. Minimum surface pressure at maximum intensity with respect to sea surface temperature, mid-level moisture, and latitude.

12. Maximum rate of intensification with respect to sea surface temperature, mid-level moisture, and latitude.

13. Time to reach maximum intensity with respect to sea surface temperature, mid-level moisture, and latitude.

14. Effect of sea surface temperature on the (a) minimum surface pressure with time, and on the (b) radius of 30-knot winds in layer 0 with time.

15. Effect of mid-level moisture on the (a) minimum surface pressure with time, and on the (b) radius of 30-knot winds in layer 0 with time.

16. Effect of latitude on the (a) minimum surface pressure with time, and on the (b) radius of 30-knot winds in layer 0 with time.

17. Radius of 30-knot winds at maximum intensity with respect to sea surface temperature, mid-level moisture, and latitude.

18. Effects of sea surface temperature, mid-level moisture, and latitude on the minimum surface pressure at maximum intensity versus the rate of maximum intensification.

19. Comparisons of trends between sea surface temperature and minimum surface pressure at maximum intensity at different latitudes.

20. Comparisons of trends between sea surface temperature and the rates of maximum intensity at different latitudes.

21. Comparisons of trends between sea surface temperature and radius of 30-knot winds at maximum intensity at different latitudes.

22. Latitudinal profiles of monthly-averaged sea surface temperatures.

23. Seasonal changes in the minimum surface pressure at maximum intensity with latitude.

24. Seasonal changes in the rate of maximum intensification with latitude.

25. Seasonal changes in the radius of 30-knot winds at maximum intensity with latitude.

26. Climatology of the radius of 30-knot winds with respect to latitude.

27. Climatology of the minimum surface pressure with respect to latitude.

28. Climatology of (a) the minimum surface pressure with respect to latitude and storm size and (b) the radius of 30-knot winds with respect to latitude and SLP.

29. Climatology of (a) minimum surface pressure and (b) radius of 30-knot surface winds with respect to average rate of latitudinal movement and latitude.

30. Climatology of (a) minimum surface pressure and (b) radius of 30-knot surface winds with respect to current rate of latitudinal movement and latitude.

31. Climatology of the minimum surface pressure at (a) maximum intensity and at (b) maximum rate of surface pressure change with respect to latitude.

32. Climatology of the minimum surface pressure at (a) maximum intensity and at (b) radius of 30-knot surface winds with respect to latitude.

33. Radial distribution of the maximum vertical velocity with time and latitude.

34. Maximum radial winds versus maximum tangential winds in layer 0 with respect to time and latitude.

35. Inertial stability at radius of maximum heating with respect to latitude. The inertial stability values have been normalized by the corresponding Coriolis parameter, f.

36. The vertical stability factor, η, at maximum vertical velocity with respect to time and latitude.

LIST OF TABLES

1. Values of parameters used in the standard numerical model simulation.

2. Vertical equivalent potential temperature profiles used in testing of Ooyama's (1969) model and the study model.

1. INTRODUCTION

Tropical cyclones with their destructiveness and complexity have been the focus of numerous theoretical and observational studies. The destructiveness is a result of the intense low-level winds and the torrential rains. The complexity arises from interactions between scales of motion that are dynamically quite different, i.e. synoptic scale and cumulus convection scale. Ooyama (1964) and Charney and Eliassen (1964) have shown that circulations of these distinct scales could enhance each other by cooperative interaction, often referred to as Conditional Instability of the Second Kind (CISK).

Merrill (1985) summarized the evolving conceptual understanding of tropical cyclone structure from 1900 to 1980. From 1900 to 1957 the large-scale structure of the storms were qualitatively studied from ground-based stations. The advent of flying instrumented aircraft into tropical cyclones and the use of computers from 1958 to 1963 brought about a concentrated study of the core of the hurricane. Most of the observational data was within 100 km of the storm center as a result of the limited flying range of the aircraft. Between 1964 and 1975, numerical modeling of tropical cyclones rapidly developed as a result of the concept of CISK and Project STORMFURY, a plan to reduce the maximum winds in a hurricane. During this time research on environmental factors essentially stopped and

the study of large-scale aspects of hurricanes was outside the mainstream of hurricane research. Interest in the large-scale aspects of tropical cyclones renewed as a result of the developments of more advanced weather reconnaissance airplanes, operational geosynchronous satellites with infrared sensors, and the combining of observations from various hurricanes into composites during 1976 and 1980. One of the major limitations of the previous research is that the primary emphasis has been on the detailed structure near the storm center rather than the full horizontal extent of the storm circulation.

Several studies have dealt with quantifying the size of tropical cyclones and analyzing environmental factors that may influence the storm size (e.g., Merrill 1982; Weatherford, 1985; Brand, 1972; and McBride and Zehr, 1981), and a few papers have noted the effect of sea surface temperature or latitude on the size of the hurricane in numerical models (Ooyama, 1969; Yamasaki, 1968). The purpose of this research is to develop a numerical model with maximum simplification that can be used to analyze the development of tropical cyclones. The model will then be used to investigate factors which affect the storm size. The results will be compared to climatology data of Air Force weather reconnaissance flights through tropical cyclones in the western Pacific during 1980 to 1982 (Weatherford, 1985).

An axisymmetric numerical model was chosen because many of the physical aspects of tropical cyclones are not critically dependent on azimuthal variations (Anthes, 1982) and the computational memory and run time of an axisymmetric model are significantly less than for a three-dimensional numerical model. One of the first axisymmetric numerical models that produced a circulation and evolution that resembled an average tropical cyclone was developed by Ooyama (1969). The model to be used in this study is similar to Ooyama's model, but is slightly more general. Both models contain a relatively simple cumulus parameterization, the minimum vertical resolution (three layers), and the simplest geometry (f-plane) which can be used for tropical cyclone simulations. The two primary modifications are that compressible fluid layers with isentropic coordinates rather than incompressible fluid layers are used and that primitive equations rather than the balance equations are used.

Another modification to Ooyama's model is that the governing equations are solved by the spectral method rather than the finite difference method. Spectral methods are much more accurate per degree of freedom compared to finite difference methods, and spectral methods can reduce computational dispersion caused by an artificial phase speed for waves with wavelengths close to twice the grid spacing in a finite difference model

(Machenhauer, 1979; DeMaria, 1983). In meteorology, the spectral method has been used in global atmospheric modeling since the early 1970s, but the method has been employed in modeling tropical cyclones since 1983 (DeMaria, 1983).

In the spectral method the spatial dependence of the dependent variables is represented by a finite series of basis functions which are orthogonal with respect to some inner product and satisfy the same boundary conditions as the dependent variables. The equations for the time dependent amplitudes are found by substituting the series expansions into the governing equations and then taking the inner product of the equations with each of the basis functions. The governing equations are then transformed into a series of ordinary differential equations for the expansion coefficients (often referred to as spectra). When these equations are solved using time differencing it is necessary to evaluate the transform of the nonlinear terms at each time step. Using the transform method (Orszag, 1970) the nonlinear terms are computed by first transforming the dependent variables to physical space on some specific grid. The nonlinear products are then calculated at the grid points and the inverse transform is evaluated using an appropriate numerical quadrature rule. The transform method makes the inclusion of physical processes straightforward since the dependent variables

are calculated in physical space at each time step. Machenhauer (1979), DeMaria (1983), and Schubert and DeMaria (1984) provide a more detailed history and description of the spectral method.

2. MODEL DESCRIPTION

2.1 Governing Equations

The governing equations for a rotating, axisymmetric hydrostatic fluid in isentropic, cylindrical coordinates can be written as:

$$\frac{\partial u}{\partial t} + u\frac{\partial u}{\partial r} + \dot{\theta}\frac{\partial u}{\partial \theta} - \frac{v^2}{r} - fv + \frac{\partial M}{\partial r} = F_u \qquad (1)$$

$$\frac{\partial v}{\partial t} + u\frac{\partial v}{\partial r} + \dot{\theta}\frac{\partial v}{\partial \theta} + \frac{uv}{r} + fu = F_v \qquad (2)$$

$$\frac{\partial M}{\partial \theta} = \Pi \qquad (3)$$

$$\frac{\partial \sigma}{\partial t} + \frac{1}{r}\frac{\partial (r\sigma u)}{\partial r} + \frac{\partial (\dot{\theta}\sigma)}{\partial \theta} = 0 \qquad (4)$$

$$\frac{d\theta}{dt} = \dot{\theta} = \frac{\dot{Q}}{\Pi} \qquad (5)$$

$$\sigma = -\frac{\partial P}{\partial \theta} \qquad (6)$$

$$\Pi = c_p (p/p_0)^{K} \qquad (7)$$

$$M = c_p T + \phi = \theta\Pi + \phi \qquad (8)$$

where: u = radial component of the wind

v = tangential component of the wind

θ = potential temperature

$\dot{\theta} = \frac{\partial \theta}{\partial t}$ = vertical velocity

f = Coriolis parameter

t = time

r = radial distance from the storm center

F_u & F_v = friction terms

σ = pseudo-density

M = Montgomery stream function

Π = Exner function

p = pressure (p $\approx$ 1000mb)

c_p = specific heat of dry air

$K = R_d / c_p$

T = absolute temperature

ϕ = geopotential = gz $\begin{cases} g = \text{acceleration of gravity} \\ z = \text{vertical height} \end{cases}$

Q = heating term

$\dot{Q} = \frac{dQ}{dt}$ = rate of heating

Assuming Q and F are known or parameterized, then equations (1)-(6) are six equations with independent variables r, θ, and t; and dependent variables u, v, M, σ, Π, and p.

2.2 Vertical Discretization

For upper and lower boundary conditions, assume that

$$\left.\begin{aligned} p &= p_U = \text{constant} \\ \theta &= \theta_U = \text{constant} \end{aligned}\right\} \quad \text{upper boundary (9)}$$

$$\left.\theta = \theta_L = \text{constant}\right\} \quad \text{lower boundary (10)}$$

To vertically discretize equations (1)–(8), consider a fluid which has three layers of constant potential temperature as shown in Figure 1.

At $z = 0$, $M = \theta\Pi$ so

$$M_0 = \theta_0 \Pi_s \tag{11}$$

Integrating equation (3) across the interfaces between layers 0–1 and 1–2 gives:

$$M_1 = M_0 + (\theta_1 - \theta_0)\Pi_{1/2} \tag{12}$$

$$M_2 = M_1 + (\theta_2 - \theta_1)\Pi_{3/2} \tag{13}$$

The momentum equations, (1)–(2) are more easily discretized when in flux form. Therefore, multiply (1) by σ and (4) by u and adding gives:

$$\frac{\partial(u\sigma)}{\partial t} + \frac{1}{r}\frac{\partial(u^2 r\sigma)}{\partial r} + \frac{\partial(u\sigma\dot{\theta})}{\partial\theta} - \frac{\sigma v^2}{r} - \sigma f v + \frac{\partial M}{\partial r} = \sigma F_u \tag{14}$$

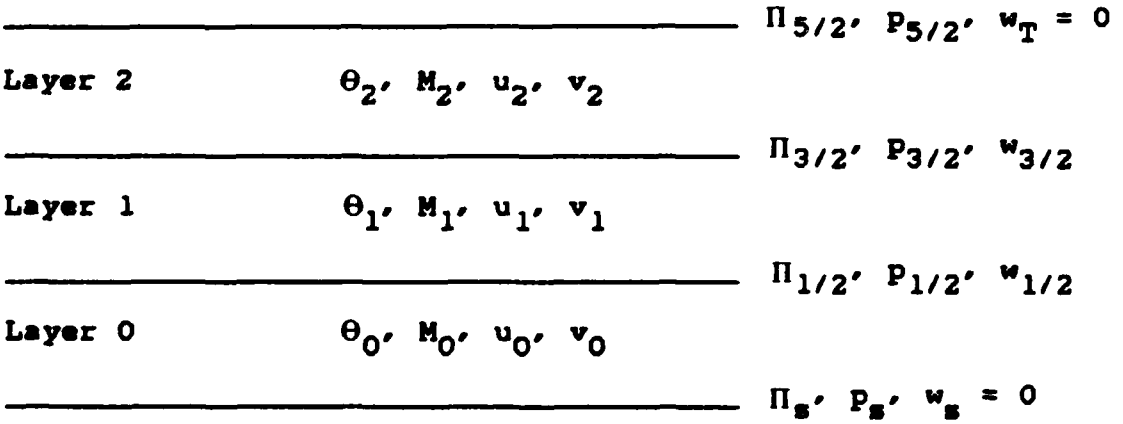

Figure 1 Schematic representation of the three layers of the numerical simulation and the notation of the basic dependent variables.

and multiplying (2) by σ and (4) by v and adding gives:

$$\frac{\partial(v\sigma)}{\partial t} + \frac{1}{r}\frac{\partial(uvr\sigma)}{\partial r} + \frac{\partial(v\sigma\dot{\theta})}{\partial\theta} + \frac{\sigma uv}{r} + \sigma f u = \sigma F_v \qquad (15)$$

Since θ is constant in each layer, then, from (3), M will also be vertically constant in each layer. Since the pressure gradient force is constant in the vertical for each layer, it is also assumed that u and v are also vertically constant in each layer.

Vertically integrating (14) and (15) across layers 0, 1, and 2 gives:

$$\frac{\partial(u_0 \Delta p_0)}{\partial t} + \frac{1}{r}\frac{\partial(u_0^2 r \Delta p_0)}{\partial r} + \overset{+}{w}_{1/2}u_0 - \overset{-}{w}_{1/2}u_1 - \frac{\Delta p_0 v_0^2}{r}$$

$$- \Delta p_0 f v_0 + \Delta p_0 \frac{\partial M_0}{\partial r} = \Delta p_0 F_{u0} \qquad (16a)$$

$$\frac{\partial(u_1 \Delta p_1)}{\partial t} + \frac{1}{r}\frac{\partial(u_1^2 r \Delta p_1)}{\partial r} + \overset{+}{w}_{3/2}u_1 - \overset{-}{w}_{3/2}u_2 - \overset{+}{w}_{1/2}u_0$$

$$+ \overset{-}{w}_{1/2}u_1 - \frac{\Delta p_1 v_1^2}{r} - \Delta p_1 f v_1 + \Delta p_1 \frac{\partial M_1}{\partial r} = \Delta p_1 F_{u1} \qquad (16b)$$

$$\frac{\partial(u_2 \Delta p_2)}{\partial t} + \frac{1}{r}\frac{\partial(u_2^2 r \Delta p_2)}{\partial r} - \overset{+}{w}_{3/2}u_1 + \overset{-}{w}_{3/2}u_2 - \frac{\Delta p_2 v_2^2}{r}$$

$$-\Delta p_2 f v_2 + \Delta p_2 \frac{\partial M_2}{\partial r} = \Delta p_2 F_{u2} \qquad (16c)$$

$$\frac{\partial(v_0\Delta p_0)}{\partial t} + \frac{1}{r}\frac{\partial(u_0 v_0 \Delta p_1 r)}{\partial r} + \overset{+}{w}_{1/2}v_0 - \overset{-}{w}_{1/2}v_1 + \frac{\Delta p_0 u_0 v_0}{r} \tag{17a}$$

$$+\Delta p_0 f u_0 = \Delta p_0 F_{v0}$$

$$\frac{\partial(v_1\Delta p_2)}{\partial t} + \frac{1}{r}\frac{\partial(u_1 v_1 \Delta p_1 r)}{\partial r} + \overset{+}{w}_{3/2}v_1 - \overset{-}{w}_{3/2}v_2 - \overset{+}{w}_{1/2}v_0 \tag{17b}$$

$$+ \overset{-}{w}_{1/2}v_1 + \frac{\Delta p_1 u_1 v_1}{r} + \Delta p_1 f u_1 = \Delta p_1 F_{v1}$$

$$\frac{\partial(v_2\Delta p_2)}{\partial t} + \frac{1}{r}\frac{\partial(u_2 v_2 \Delta p_2 r)}{\partial r} - \overset{+}{w}_{3/2}v_1 + \overset{-}{w}_{3/2}v_2 + \frac{\Delta p_2 u_2 v_2}{r} \tag{17c}$$

$$+\Delta p_2 f u_2 = \Delta p_2 F_{v2}$$

where: $$w = \sigma\dot{\theta} \tag{18}$$

$$w^+ = \frac{1}{2}(|w| + w) \quad , \quad w^- = \frac{1}{2}(|w| - w) \tag{19}$$

$$\Delta p_j = p_{j-1/2} - p_{j+1/2} \quad \text{and} \quad p_s = p_{-1/2} \tag{20}$$

Note that $\dot{\theta}$ is assumed to be zero at the surface and at the upper boundary.

Integrating (4) across each layer gives:

$$\frac{\partial(\Delta p_0)}{\partial t} + \frac{1}{r}\frac{\partial(r u_0 \Delta p_0)}{\partial r} + w_{1/2} = 0 \tag{21}$$

$$\frac{\partial(\Delta p_1)}{\partial t} + \frac{1}{r}\frac{\partial(r u_1 \Delta p_1)}{\partial r} + w_{3/2} - w_{1/2} = 0 \qquad (22)$$

$$\frac{\partial(\Delta p_2)}{\partial t} + \frac{1}{r}\frac{\partial(r u_2 \Delta p_2)}{\partial r} - w_{3/2} = 0 \qquad (23)$$

where: $w = w^+ - w^-$

Once the equations are vertically discretized, it is more convenient to work with the momentum equations in advective form. Multiplying (21) by u_0 and subtracting from (16a), and multiplying (21) by v_0 and subtracting from (17a) gives:

$$\frac{\partial u_0}{\partial t} + u_0\frac{\partial u_0}{\partial r} + \frac{\bar{w}_{1/2}(u_0 - u_1)}{\Delta p_0} - \frac{v_0^2}{r} - f v_0 + \frac{\partial M_0}{\partial r} = F_{u0} \qquad (24)$$

$$\frac{\partial v_0}{\partial t} + u_0\frac{\partial v_0}{\partial r} + \frac{\bar{w}_{1/2}(v_0 - v_1)}{\Delta p_0} + \frac{u_0 v_0}{r} + f u_0 = F_{v0} \qquad (25)$$

The results are similar for layers 1 and 2.

Provided that w^+, w^-, and F are known, then (11)-(13), (21)-(25) form a closed system if the p_j quantities can be related to M_j.

Defining

$$\Delta\theta_s = \theta_0$$

$$\Delta\theta_{1/2} = \theta_1 - \theta_0 \qquad (26)$$

$$\Delta\theta_{3/2} = \theta_2 - \theta_1$$

then, from (11)-(13),

$$M_0 = \Delta\theta_s \Pi_s$$

$$M_1 = \Delta\theta_{s\ s} + \Delta\theta_{1/2}\Pi_{1/2} \tag{27}$$

$$M_2 = \Delta\theta_s \Pi_s + \Delta\theta_{1/2}\Pi_{1/2} + \Delta\theta_{3/2}\Pi_{3/2}$$

From (20)

$$\Delta p_0 = p_s - p_{1/2}$$

$$\Delta p_1 = p_{1/2} - p_{3/2} \tag{28}$$

$$\Delta p_2 = p_{3/2} - p_T$$

and so,

$$p_{3/2} = \Delta p_2 + p_T$$

$$p_{1/2} = \Delta p_2 + \Delta p_1 + p_T \tag{29}$$

$$p_s = \Delta p_2 + \Delta p_1 + \Delta p_0 + p_T$$

Now, from the chain rule,

$$\frac{\partial \Pi_s}{\partial r} = \frac{d\Pi_s}{dp}\frac{\partial p_s}{\partial r}$$

$$\frac{\partial \Pi_{1/2}}{\partial r} = \frac{d\Pi_{1/2}}{dp}\frac{\partial p_{1/2}}{\partial r} \tag{30}$$

$$\frac{\partial \Pi_{3/2}}{\partial r} = \frac{d\Pi_{3/2}}{dp}\frac{\partial p_{3/2}}{\partial r}$$

Defining the static stability, Γ,

$$\Gamma_{j-1/2} = \frac{d\Pi_{j-1/2}}{dp} = \frac{K\, c_p}{p_{j-1/2}} \left(\frac{p_{j-1/2}}{p_0} \right)^K \qquad j=0,1,2 \qquad (31)$$

where $\Gamma_s = \Gamma_{-1/2}$

then from (30) and (31)

$$\frac{\partial \Pi_s}{\partial r} = \Gamma_s \frac{\partial(\Delta p_0 + \Delta p_1 + \Delta p_2)}{\partial r}$$

$$\frac{\partial \Pi_{1/2}}{\partial r} = \Gamma_{1/2} \frac{\partial(\Delta p_1 + \Delta p_2)}{\partial r} \qquad (32)$$

$$\frac{\partial \Pi_{3/2}}{\partial r} = \Gamma_{3/2} \frac{\partial(\Delta p_2)}{\partial r}$$

Defining γ as

$$\gamma_{j-1/2} = \Gamma_{j-1/2}\, \Delta\theta_{j-1/2} \qquad j=0,1,2 \qquad (33)$$

where $\gamma_s = \gamma_{-1/2}$,

then differentiating (27) with respect to r and using (32) and (33) gives:

$$\frac{\partial M_0}{\partial r} = \gamma_s \frac{\partial(\Delta p_0 + \Delta p_1 + \Delta p_2)}{\partial r}$$

$$\frac{\partial M_1}{\partial r} = \gamma_s \frac{\partial(\Delta p_0)}{\partial r} + (\gamma_s + \gamma_{1/2}) \frac{\partial(\Delta p_1 + \Delta p_2)}{\partial r} \qquad (34)$$

$$\frac{\partial M_2}{\partial r} = \gamma_s \frac{\partial(\Delta p_0)}{\partial r} + (\gamma_s + \gamma_{1/2}) \frac{\partial(\Delta p_1)}{\partial r} + (\gamma_s + \gamma_{1/2} + \gamma_{3/2}) \frac{\partial(\Delta p_2)}{\partial r} \quad (34 \text{ cont.})$$

It is convenient to divide γ_j into a mean part $\bar{\gamma}_j$ calculated from constant pressure, $\bar{P}_j$, and a perturbation part γ_j' where

$$\gamma_j = \bar{\gamma}_j + \gamma_j' \quad (35)$$

Now, define

$$\Delta p_0 = \frac{g}{\bar{\gamma}_s} \epsilon_0 h_0$$

$$\Delta p_1 = \frac{g}{\bar{\gamma}_s} \epsilon_1 h_1 \quad (36)$$

$$\Delta p_2 = \frac{g}{\bar{\gamma}_s} \epsilon_2 h_2$$

$$\epsilon_0 = \bar{\gamma}_s / \bar{\gamma}_s = 1 \qquad \beta_0 = \bar{\gamma}_s / \gamma_s'$$

$$\epsilon_1 = \bar{\gamma}_s / (\bar{\gamma}_s + \bar{\gamma}_{1/2}) \qquad \beta_1 = \bar{\gamma}_s / (\gamma_s' + \gamma_{1/2}') \quad (37)$$

$$\epsilon_2 = \bar{\gamma}_s / (\bar{\gamma}_s + \bar{\gamma}_{1/2} + \bar{\gamma}_{3/2}) \qquad \beta_2 = \bar{\gamma}_s / (\gamma_s' + \gamma_{1/2}' + \gamma_{3/2}')$$

where ϵ_j represent static stability factors of the mean atmosphere, the inverse of β_j represent static stability change due to deviations from the basic state of the atmosphere, and the factors are proportional to h_j the thickness of the layers.

Using (35) and (36), (34) can be written as

$$\frac{\partial M_0}{\partial r} = g\frac{\partial(h_0 + \epsilon_1 h_1 + \epsilon_2 h_2)}{\partial r} + \frac{g}{\beta_0}\frac{\partial(h_0 + \epsilon_1 h_1 + \epsilon_2 h_2)}{\partial r}$$

$$\frac{\partial M_1}{\partial r} = g\frac{\partial(h_0 + h_1 + (\epsilon_2/\epsilon_1)h_2)}{\partial r} + \frac{g}{\beta_0}\frac{\partial h_0}{\partial r} + \frac{g}{\beta_1}\frac{\partial(\epsilon_1 h_1 + \epsilon_2 h_2)}{\partial r} \qquad (38)$$

$$\frac{\partial M_2}{\partial r} = g\frac{\partial(h_0 + h_1 + h_2)}{\partial r} + \frac{g}{\beta_0}\frac{\partial h_0}{\partial r} + \frac{g}{\beta_1}\frac{\partial(\epsilon_1 h_1)}{\partial r} + \frac{g}{\beta_2}\frac{\partial(\epsilon_2 h_2)}{\partial r}$$

Since ϵ_j and β_j are nondimensional, h_j have the dimensions of length.

Define the heating term, Q, as

$$Q_{j-1/2} = \frac{\bar{\gamma}_s w_{j-1/2}}{g} \qquad j=1,2 \qquad (39)$$

Φ as

$$\Phi_0 = \frac{g}{\beta_0}\frac{\partial(h_0 + \epsilon_1 h_1 + \epsilon_2 h_2)}{\partial r}$$

$$\Phi_1 = \frac{g}{\beta_0}\frac{\partial h_0}{\partial r} + \frac{g}{\beta_1}\frac{\partial(\epsilon_1 h_1 + \epsilon_2 h_2)}{\partial r} \qquad (40)$$

$$\Phi_2 = \frac{g}{\beta_0}\frac{\partial h_0}{\partial r} + \frac{g}{\beta_1}\frac{\partial(\epsilon_1 h_1)}{\partial r} + \frac{g}{\beta_2}\frac{\partial(\epsilon_2 h_2)}{\partial r}$$

and the geopotential, ϕ, as

$$\phi_0 = g(h_0 + \epsilon_1 h_1 + \epsilon_2 h_2)$$

$$\phi_1 = g(h_0 + h_1 + (\epsilon_2/\epsilon_1)h_2) \qquad (41)$$

$$\Phi_2 = g\,(h_0 + h_1 + h_2) \qquad \text{(41 cont.)}$$

then (24) can be written as

$$\frac{\partial u_0}{\partial t} + u_0\frac{\partial u_0}{\partial r} + \frac{\bar{Q}_{1/2}}{h_0}(u_0 - u_1) - \frac{v_0^2}{r} - fv_0 + \frac{\partial \phi_0}{\partial r} = -\Phi_0 + F_{u0}$$

$$\frac{\partial u_1}{\partial t} + u_1\frac{\partial u_1}{\partial r} + \frac{\bar{Q}_{3/2}}{\epsilon_1 h_1}(u_1 - u_2) + \frac{\overset{+}{Q}_{3/2}}{\epsilon_1 h_1}(u_1 - u_0) - \frac{v_1^2}{r} - fv_1 + \frac{\partial \phi_1}{\partial r} = -\Phi_1 + F_{u1} \qquad (42)$$

$$\frac{\partial u_2}{\partial r} + u_2\frac{\partial u_2}{\partial r} + \frac{\overset{+}{Q}_{3/2}}{\epsilon_2 h_2}(u_2 - u_1) - \frac{v_2^2}{r} - fv_2 + \frac{\partial \phi_2}{\partial r} = -\Phi_2 + F_{u2}$$

and (25) can be written as

$$\frac{\partial v_0}{\partial t} + u_0\frac{\partial v_0}{\partial r} + \frac{\bar{Q}_{1/2}}{h_0}(v_0 - v_1) + \frac{u_0 v_0}{r} + fu_0 = F_{v0}$$

$$\frac{\partial v_1}{\partial t} + u_1\frac{\partial v_1}{\partial r} + \frac{\bar{Q}_{3/2}}{\epsilon_1 h_1}(v_1 - v_2) + \frac{\overset{+}{Q}_{3/2}}{\epsilon_1 h_1}(v_1 - v_0) + \frac{u_1 v_1}{r} + fu_1 = F_{v1} \qquad (43)$$

$$\frac{\partial v_2}{\partial t} + u_2\frac{\partial v_2}{\partial r} + \frac{\overset{+}{Q}_{3/2}}{\epsilon_2 h_2}(v_2 - v_1) + \frac{u_2 v_2}{r} + fu_2 = F_{v2}$$

Similarly, using (35) and (39), (21)-(23) can be written as

$$\frac{\partial h_0}{\partial t} + \frac{1}{r}\frac{\partial (r u_0 h_0)}{\partial r} + Q_{1/2} = 0$$

$$\frac{\partial h_1}{\partial t} + \frac{1}{r}\frac{\partial (r u_1 h_1)}{\partial r} + \frac{Q_{3/2}}{\epsilon_1} - \frac{Q_{1/2}}{\epsilon_2} = 0 \qquad (44)$$

$$\frac{\partial h_2}{\partial t} + \frac{1}{r}\frac{\partial (r u_2 h_2)}{\partial r} - \frac{Q_{3/2}}{\epsilon_2} = 0$$

Let $h_j = H_j + h'_j$ where H_j represents the average thickness of layer j and h'_j the perturbation thickness of layer j, and noting that

$$u_j \frac{\partial u_j}{\partial r} = \frac{u_j}{r}\frac{\partial (r u_j)}{\partial r} - \frac{u_j^2}{r}$$

then the equations of motion can be written as:

$$\frac{\partial u_0}{\partial t} - f v_0 + \frac{\partial \phi_0}{\partial r} = -\Phi_0 - \frac{u_0}{r}\frac{\partial (r u_0)}{\partial r} + \frac{u_0^2 + v_0^2}{r} - \frac{Q_{1/2}(u_1 - u_0)}{(H_0 + h_0')} + F_{u0}$$

$$\frac{\partial u_1}{\partial t} - f v_1 + \frac{\partial \phi_1}{\partial r} = -\Phi_1 - \frac{u_1}{r}\frac{\partial (r u_1)}{\partial r} + \frac{u_1^2 + v_1^2}{r} + \frac{Q_{1/2}(u_0 - u_1)}{\epsilon_1 (H_1 + h_1')} - \frac{Q_{3/2}(u_2 - u_1)}{\epsilon_1 (H_1 + h_1')} + F_{u1} \qquad (45)$$

$$\frac{\partial u_2}{\partial t} - fv_2 + \frac{\partial \phi_2}{\partial r} = -\Phi_2 - \frac{u_2}{r}\frac{\partial (ru_2)}{\partial r} + \frac{u_2^2 + v_2^2}{r}$$

(45 cont.)

$$+ \frac{\overset{+}{Q}_{3/2}(u_1 - u_2)}{\epsilon_2(H_2 + h_2')} + F_{u2}$$

$$\frac{\partial v_0}{\partial t} + fu_0 = -\frac{u_0}{r}\frac{\partial (rv_0)}{\partial r} + \frac{\overset{-}{Q}_{1/2}(v_1 - v_0)}{(H_0 + h_0')} + F_{v0}$$

$$\frac{\partial v_1}{\partial t} + fu_1 = -\frac{u_1}{r}\frac{\partial (rv_1)}{\partial r} + \frac{\overset{+}{Q}_{1/2}(v_0 - v_1)}{\epsilon_1(H_1 + h_1')}$$

$$+ \frac{\overset{-}{Q}_{3/2}(v_2 - v_1)}{\epsilon_1(H_1 + h_1')} + F_{v1} \qquad (46)$$

$$\frac{\partial v_2}{\partial t} + fu_2 = -\frac{u_2}{r}\frac{\partial (rv_2)}{\partial r} + \frac{\overset{+}{Q}_{3/2}(v_1 - v_2)}{\epsilon_2(H_2 + h_2')} + F_{v2}$$

$$\frac{\partial h_0'}{\partial t} + H_0\frac{\partial (ru_0)}{r\,\partial r} = -u_0\frac{\partial h_0'}{\partial r} - h_0'\frac{\partial (ru_0)}{r\,\partial r} - \overset{+}{Q}_{1/2} + \overset{-}{Q}_{1/2}$$

$$\frac{\partial h_1'}{\partial t} + H_1\frac{\partial (ru_1)}{r\,\partial r} = -u_1\frac{\partial h_1'}{\partial r} - h_1'\frac{\partial (ru_1)}{r\,\partial r} + \frac{\overset{+}{Q}_{1/2}}{\epsilon_1} - \frac{\overset{-}{Q}_{1/2}}{\epsilon_1}$$

(47)

$$- \frac{\overset{+}{Q}_{3/2}}{\epsilon_1} + \frac{\overset{-}{Q}_{3/2}}{\epsilon_1}$$

$$\frac{\partial h_2'}{\partial t} + H_2\frac{\partial (ru_2)}{r\,\partial r} = -u_2\frac{\partial h_2'}{\partial r} - h_2'\frac{\partial (ru_2)}{r\,\partial r} + \frac{\overset{+}{Q}_{3/2}}{\epsilon_2} - \frac{\overset{-}{Q}_{3/2}}{\epsilon_2}$$

where Φ_j and ϕ_j are defined in equations (40) and (41), respectively. Note that the equations for a rotating axisymmetric fluid in isentropic, cylindrical coordinates are similar to the equations presented by Ooyama (1969) for an atmosphere with three incompressible fluid layers. The only differences are that the Φ_j terms do not appear in the incompressible fluid layer model, and Ooyama's model uses the balance approximation.

In this 3-layer model structure, θ_0, θ_1, θ_2, and P_T are specified constants. It is also necessary to specify the basic state pressures $\bar{P}_s$, $\bar{P}_{1/2}$, and $\bar{P}_{3/2}$. Once these values are specified, the constants H_0, H_1, H_2, ϵ_1, and ϵ_2 can be calculated as follows:

$$\bar{\gamma}_s = \frac{R_d}{P_s}\left(\frac{\bar{P}_s}{P_0}\right)^K \theta_0$$

$$\bar{\gamma}_{1/2} = \frac{R_d}{P_{1/2}}\left(\frac{\bar{P}_{1/2}}{P_0}\right)^K (\theta_1 - \theta_0) \qquad (48)$$

$$\bar{\gamma}_{3/2} = \frac{R_d}{P_{3/2}}\left(\frac{\bar{P}_{3/2}}{P_0}\right)^K (\theta_2 - \theta_1)$$

$$\begin{aligned} \epsilon_0 &= 1 \\ \epsilon_1 &= \bar{\gamma}_s / (\bar{\gamma}_s + \bar{\gamma}_{1/2}) \\ \epsilon_2 &= \bar{\gamma}_s / (\bar{\gamma}_s + \bar{\gamma}_{1/2} + \bar{\gamma}_{3/2}) \end{aligned} \qquad (49)$$

$$H_0 = \frac{(\bar{p}_s - \bar{p}_{1/2})\bar{\gamma}_s}{g}$$

$$H_1 = \frac{(\bar{p}_{1/2} - \bar{p}_{3/2})\bar{\gamma}_s}{g} \qquad (50)$$

$$H_2 = \frac{(\bar{p}_{3/2} - \bar{p}_T)\bar{\gamma}_s}{g}$$

The β_j terms in (40) are calculated from h'_0, h'_1, and h'_2 and the following equations:

$$p_{3/2} = p_T + \frac{g\epsilon_2}{\bar{\gamma}_s}(H_2 + h_2') = \bar{p}_{3/2} + \frac{g\epsilon_2}{\bar{\gamma}_s}(h_2')$$

$$p_{1/2} = p_{3/2} + \frac{g\epsilon_1}{\bar{\gamma}_s}(H_1 + h_1') = \bar{p}_{1/2} + \frac{g}{\bar{\gamma}_s}(\epsilon_1 h_1' + \epsilon_2 h_2') \qquad (51)$$

$$p_s = p_{1/2} + \frac{g}{\bar{\gamma}_s}(H_0 + h_0') = \bar{p}_s + \frac{g}{\bar{\gamma}_s}(h_0' + \epsilon_1 h_1' + \epsilon_2 h_2')$$

$$\gamma_s = \frac{R_d}{p_s}\left(\frac{p_s}{p_0}\right)^K \qquad \gamma_s' = \gamma_s - \bar{\gamma}_s$$

$$\gamma_{1/2} = \frac{R_d}{p_{1/2}}\left(\frac{p_{1/2}}{p_0}\right)^K(\theta_1 - \theta_0) \qquad \gamma_{1/2}' = \gamma_{1/2} - \bar{\gamma}_{1/2} \qquad (52)$$

$$\gamma_{3/2} = \frac{R_d}{p_{1/2}}\left(\frac{p_{3/2}}{p_0}\right)^K(\theta_2 - \theta_1) \qquad \gamma_{3/2}' = \gamma_{3/2} - \bar{\gamma}_{3/2}$$

$$\beta_0' = \bar{\gamma}_s / \gamma_s'$$

$$\beta_1' = \bar{\gamma}_s /(\gamma_s' + \gamma_{1/2}') \qquad (53)$$

$$\beta_2' = \bar{\gamma}_s /(\gamma_s' + \gamma_{1/2}' + \gamma_{3/2}')$$

2.3 Parameterization of Physical Processes

In order to close the system of equations, (40)-(41) and (45)-(53), the F terms and the diabatic terms, $Q_{1/2}$ and $Q_{3/2}$, must be parameterized in terms of other dependent variables.

To parameterize $\vec{F}$, the surface drag, horizontal eddy diffusion of momentum, and the vertical shear between the layer interfaces are considered. The F terms in equations (54) are written as (DeMaria and Schubert, 1984):

$$\vec{F}_0 = -\frac{C_D}{H_0}|\vec{V}_0|\vec{V}_0 + \lambda_2(\nabla^2 - \frac{1}{r^2})\vec{V}_0 - \mu\frac{(\vec{V}_1-\vec{V}_2)}{(H_0 + h_0')}$$

$$\vec{F}_1 = \lambda_2(\nabla^2 - \frac{1}{r^2})\vec{V}_1 - \frac{\mu(\vec{V}_1-\vec{V}_2)}{\epsilon_1(H_1+h_1')} + \frac{\mu(\vec{V}_0-\vec{V}_1)}{\epsilon_1(H_1+h_1')} \qquad (54)$$

$$\vec{F}_2 = \lambda_2(\nabla^2 - \frac{1}{r^2})\vec{V}_2 + \frac{\mu(\vec{V}_1-\vec{V}_2)}{\epsilon_2(H_2+h_2')}$$

(A) (B) (C)

where $|\vec{V}_0|$ represents the magnitude of the boundary layer horizontal velocity. Term (A) represents the surface drag

calculated from the bulk aerodynamic formula. As in DeMaria and Schubert (1984) and Ooyama (1969), the drag coefficient C_D is assumed to have constant value of 0.0015. Terms (B) represent horizontal eddy diffusion of momentum. The horizontal eddy diffusion coefficient was assumed to have a constant value of 10^3 m^2/s, as in DeMaria and Schubert (1984). Terms (C) result from vertical diffusion caused by velocity shear across the interface between layers 0 and 1 and layers 1 and 2.

To parameterize $Q_{1/2}$, assume that the pressure thickness of the boundary layer (layer 0) remains constant with time so that $dh/dt = 0$. Then from (47),

$$\overset{-}{Q}_{1/2} - \overset{+}{Q}_{1/2} = (H_0 + h_0') \frac{\partial(ru_0)}{r\,\partial r} \qquad (57)$$

Since $\overset{-}{Q}_{1/2}$ and $\overset{+}{Q}_{1/2}$ are always positive, then

$$\overset{-}{Q}_{1/2} = \begin{cases} 0 & \delta_0 \leq 0 \\ \delta_0(H_0 + h_0') & \delta_0 > 0 \end{cases}$$

$$\overset{+}{Q}_{1/2} = \begin{cases} -\delta_0(H_0 + h_0') & \delta_0 < 0 \\ 0 & \delta_0 \geq 0 \end{cases} \qquad (58)$$

where $\delta_0 = \frac{1}{r}\frac{\partial(ru_0)}{\partial r}$ = horizontal divergence in layer 0.

Parameterizing $\overset{+}{Q}_{1/2}$ and $\overset{-}{Q}_{1/2}$ using (58) indicates

that all of the mass which converges in layer 0 is transported to layer 1 by diabatic heating and that mass divergence in layer 0 is replaced by mass from layer 1 due to diabatic cooling.

To parameterize $Q^{+}_{3/2}$, assume that this term represents diabatic heating due to cumulus convection. Since sustained cumulus convection requires boundary layer moisture convergence, then assume that

$$Q^{+}_{3/2} = Q^{+}_{1/2} \tag{59}$$

Equation (59) indicates that for each unit mass of air transported from layer 0 to layer 1, η units of mass are transported to layer 2. Ooyama (1969) noted that η is a measure of instability of deep convection that includes the stabilizing effect of the warm core and the variation of equivalent potential temperature in the planetary boundary layer (layer 0). The moist static energy (S^{*}_{2}) of the saturated cloud air which reaches layer 2 is given by:

$$S_2^{*} = \frac{S_0 + (\eta - 1)S_1}{\eta} \tag{60}$$

where $S = c_pT + gz + Lq = M + Lq$ (61)

$S^{*} = c_pT + gz + Lq^{*} = M + Lq^{*}$ (62)

S = moist static energy of unsaturated air

S^{*} = moist static energy of saturated air

L = latent heat of vaporization

q = mixing ratio of unsaturated air

q^* = mixing ratio of saturated air (saturated mixing ratio)

η = vertical stability parameter

Solving (60) for η gives:

$$\eta = \frac{S_0 - S_1}{S_2^* - S_1} = 1 + \frac{S_0 - S_2^*}{S_2^* - S_1} \tag{63}$$

The Montgomery stream functions in (61)-(62) can be calculated using the following derived from (7) and (27):

$$M_0 = c_p \theta_0 \left(\frac{p_s}{p_0}\right)^K$$

$$M_1 = M_0 + c_p(\theta_1 - \theta_0)\left(\frac{p_{1/2}}{p_0}\right)^K \tag{64}$$

$$M_2 = M_1 + c_p(\theta_2 - \theta_1)\left(\frac{p_{3/2}}{p_0}\right)^K$$

The Montgomery stream functions which appear in the definitions of S_1 and S_2^* do not represent the values of M in the model layers, but rather represent M at the pressure levels of entrainment PRE and detrainment PRD. These are linearly interpolated from the M values of the model layers assuming that these are representative of the value of M at the pressure of the mid-points of each layer P_L and P_U which are given by:

$$p_L = (p_{1/2} + p_{3/2}) / 2$$
$$p_U = (p_{3/2} + p_T) / 2 \qquad (65)$$

Let the Montgomery stream functions at p_L and p_U be M_1 and M_2, and the Montgomery stream functions at PRE and PRD be M_E and M_D. Then M_E and M_D are linearly interpolated from p_L and p_U by the following:

$$M_E = M_1 + \frac{(M_2 - M_1)}{(p_L - p_U)}(p_L - PRE)$$
$$M_D = M_1 + \frac{(M_2 - M_1)}{(p_L - p_U)}(p_L - PRD) \qquad (67)$$

Then the moist static energies are calculated using:

$$S_0 = M_0 + Lq_0$$
$$S_1 = M_E + Lq_1 \qquad (68)$$
$$S_2^* = M_D + Lq_2^*$$

The moisture values q_1 and q^*_2 could be calculated at each time step. However, the variations of Lq_1 and Lq^*_2 are not large compared to changes in S_1 and S^*_2, respectively, and so q_1 and q^*_2 will be held constant. Variations of the boundary layer moisture, q_0, however, can be large. For this reason, q_0 is predicted using the following conservation equation:

$$\frac{\partial q_0}{\partial t} + u_0\frac{\partial q_0}{\partial r} + \frac{\bar{Q}_{1/2}(q_0 - q_1)}{(H_0 + h_0')} = \frac{C_E|\vec{V}_0|}{(H_0 + h_0')}(q_s - q_0) \quad (69)$$

where q_s is the saturation mixing ratio at T_{ss} and p_s; T_{ss} being the sea surface temperature, and p_s the surface pressure. Although M_0 is a function of p_s, it can be seen from (64) that M_0 will decrease as p_s decreases. Observations show that as a storm intensifies, the temperature at the surface remains approximately constant despite the decrease in the surface pressure. This is due to the sensible heat flux from the ocean surface. Since it is assumed that $\dot{\theta} = 0$ at $z = 0$, the surface sensible heat flux cannot be included in the isentropic coordinate model. The use of the predicted M_0 might then lead to artificially low values of S_0. To compensate for the lack of surface sensible heat flux in the model, the value of M_0 of the reference state, $\bar{M}_0$, will be used in the calculation of S_0 rather than the predicted value. Then

$$S_0 = \bar{M}_0 + Lq_0 \quad (70)$$

where

$$\bar{M}_0 = c_p\theta_0\left(\frac{\bar{p}_s}{p_0}\right)^K \quad (71)$$

The remaining term to be parameterized is $\bar{Q}_{3/2}$. This term represents radiative cooling. If F_{CLR} and F_{CLD} represent typical radiative cooling rates in clear and cloudy regions, respectively, then

zero- or first-order modified Bessel function of the first kind for the u, v, and h' variables or zero- or Bessel functions for the q_0 variable. The type of basis function used is dependent upon the lateral boundary conditions (DeMaria, 1983). In this case, for determining the basis functions for u, v, and h', geostrophic balance is assumed at r = a, the outer boundary of the model, and u = v = 0 at r = 0, the center of the storm. The lateral boundary conditions for q_0 are that the radial gradients of q_0 are zero at r = 0 and a.

Once the horizontal transform has been applied, the governing equations are solved using second-order Adams-Bashforth time differencing with an initial forward time step. In the simulations presented in the following sections, the horizontal series are truncated at N = 32 with a = 800 km. The nonlinear terms of the governing equations were calculated using the transform method (Orszag, 1970; Eliasen et al, 1970) using 3N + 5 evenly spaced grid points. Therefore, the spacing of the transform grid is 8 km.

DeMaria and Schubert (1984) and Machenhauer (1979) described the phenomenon of spectral blocking and the use of linear diffusion terms to mitigate the errors associated with it. Spectral blocking is a result of the higher wavenumbers of the truncated spectral series increasing in energy caused by the steepening gradients of the dependent

variables near the storm center. In this study it was found that linear diffusion terms of the form $K_H \nabla^4$ effectively inhibited spectral blocking. Terms of this form with $K_H = 1.671 \times 10^{13}$ m^4/s^2 were added to all of the prognostic governing equations. In a simple one-dimensional diffusion problem, the amplitude of highest mode in a Fourier series with 32 modes on an 800 km periodic domain decreases by a factor of e in 4 minutes using this form of diffusion.

2.5 Initial Conditions

The initial mass and wind fields for all simulations run in the study are given by:

$$u_j = 0 \qquad j = 0,1,2 \qquad (73)$$

$$v = \begin{cases} 2v_m \dfrac{r_j}{r_m}\left[1 + \left(\dfrac{r_j}{r_m}\right)^2\right]^{-1} & j = 0,1 \\ 0 & j = 2 \end{cases} \qquad (74)$$

$$\phi_j = \begin{cases} -2v_m\left[1 + \left(\dfrac{r_j}{r_m}\right)^2\right]^{-1} + fv_m r_m \ln\left[1 + \left(\dfrac{r_j}{r_m}\right)^2\right] & j = 0,1 \\ 0 & j = 2 \end{cases} \qquad (75)$$

where the maximum tangential wind, v_m, equal to 15.0 m/s at a radius, r_m, of 100 km. This initial condition is an axisymmetric vortex in gradient balance with no initial radial circulation. The values of v_m and r_m were chosen

after preliminary model runs showed a realistic and cost effective rate of intensification (reaching maximum intensity in approximately 4 or 5 days) and a smooth development in the radius of maximum tangential winds.

To run the model, it is necessary to specify the following parameters:

$$p_T,\ \bar{p}_{3/2},\ \bar{p}_{1/2},\ \bar{p}_s,\ \theta_2,\ \theta_1,\ \theta_0,\ \text{and}\ T_{ss};$$

and initial conditions must be specified for

$$u_0,\ u_1,\ u_2,\ v_0,\ v_1,\ v_2,\ h_0,\ h_1,\ h_2,\ \text{and}\ q_0.$$

Table 1 shows the numerical constants used in the numerical simulations. Average values, such as for q and θ, were derived from average soundings of typical tropical cyclones.

Table 1: Values of parameters in the standard numerical model simulation.

NUMBER OF NORMAL MODES	N	32
RADIUS OF STUDY	AK	800 km
TIME STEP	DT	60 s
LENGTH OF SIMULATION		5 days
SECOND-ORDER DIFFUSION	DA2	1.0×10^{3}
FOURTH-ORDER DIFFUSION	DA4	$1.671 \times 10^{+13}$
	P_0	1000 mb
	$\bar{P}_s$	1010 mb
	$\bar{P}_{1/2}$	910 mb
	$\bar{P}_{3/2}$	500 mb
	$\bar{P}_{5/2}=P_T$	150 mb
ENTRAINMENT PRESSURE LEVEL	PRE	700 mb
DETRAINMENT PRESSURE LEVEL	PRD	300 mb
	θ_0	$300^{\circ}K$
	θ_1	$315^{\circ}K$
	θ_2	$345^{\circ}K$
LATITUDE		$20^{\circ}N$
	c_p	1000 $J/kg^{\circ}K$
	K	0.2859
	g	9.8
	μ	5×10^{-4}
	C_E	0.0015
	C_D	0.0015
	q_0	20 gm/kg

Table 1 (continued)

q_1	6 gm/kg
q_2^*	0.8 gm/kg
T_{ss}	$28^{o}C$
L_v	2.5×10^{6} J/kg

3. MODEL SIMULATIONS

3.1 Typical Model Simulation

The standard model simulation, for which the effects of varying sea surface temperature, mid-level moisture, and latitude were compared, had a sea surface temperature of $28^{\circ}C$, mid-level moisture of 6 g/kg, and a latitude of $20^{\circ}N$. The model simulation represents 5 days, as did all subsequent runs. The amount of CPU time used for each run was roughly 3.5 hours on a VAX 11/750.

Figures 2 and 3 represent the radial and tangential wind profiles for layers 0, 1, and 2 at t = 0, 48, and 96 hours. Winds in layer 0 rapidly increase the first two days, level off during days 3 and 4, and decay during day 5. This corresponds to the daily minimum surface pressure trends (fig. 4). Tangential wind profiles in layer 1 are very similar to layer 0 except slightly slower. Winds in layer 2 are cyclonic near the center but become anticyclonic at distances roughly 200 to 400 km from the storm center. Radial winds in layer 0 are primarily convergent and divergent in layer 2 (fig. 5). The zones of maximum convergence in layer 0 and maximum divergence in layer 2 are between 50 to 100 km from the storm center.

Figure 6 shows the profiles of η, the vertical stability factor. Decreasing η values near the storm center and at r = 100 km are due to subsidence, which dries the boundary layer and reduces S_0. High values near r = 75

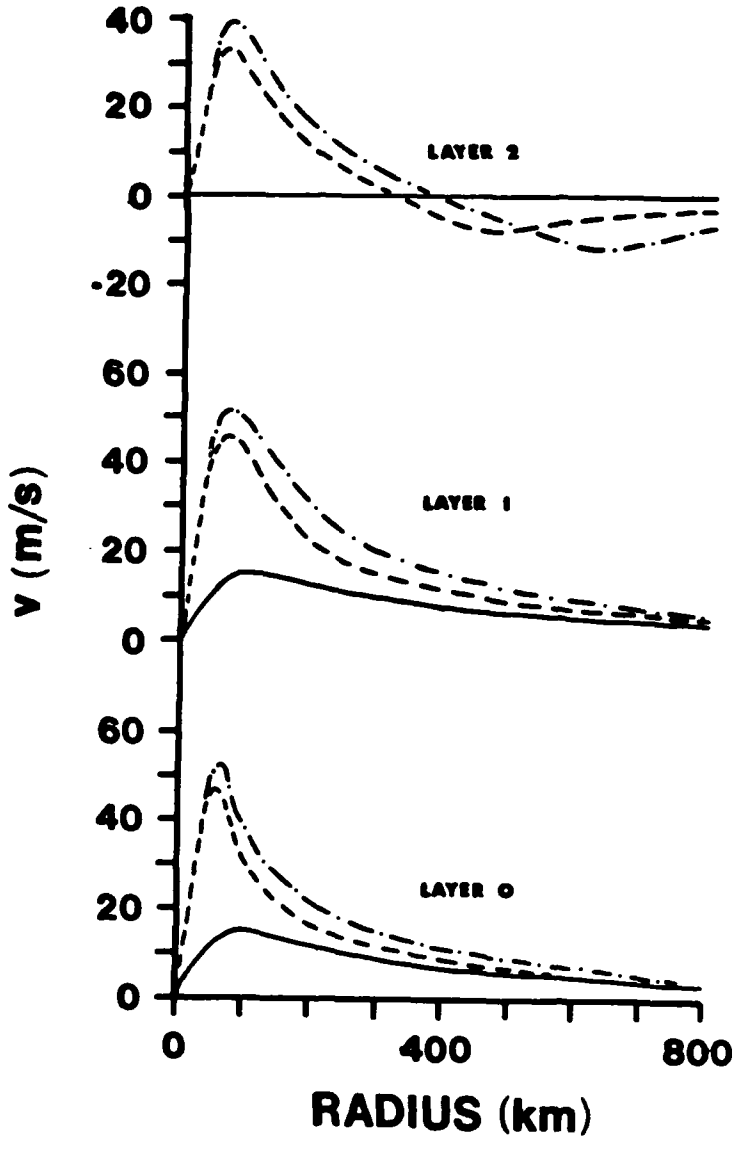

Figure 2 Profiles of tangential winds in layers 0, 1, and 2 at t = 0 (solid), 48 (dash), and 96 (dash-dot) hours.

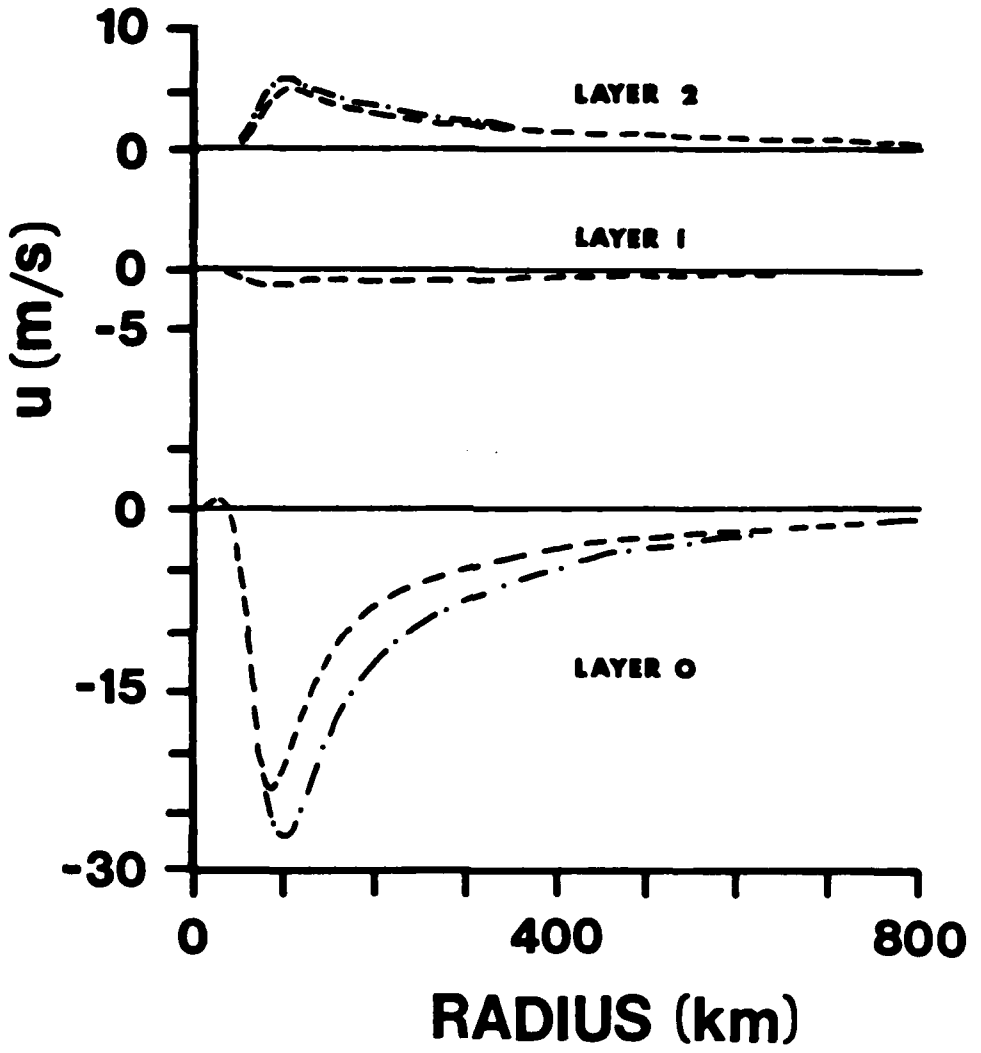

Figure 3 Profiles of radial winds in layers 0, 1, and 2 at t = 0 (solid), 48 (dash), and 96 (dash-dot) hours.

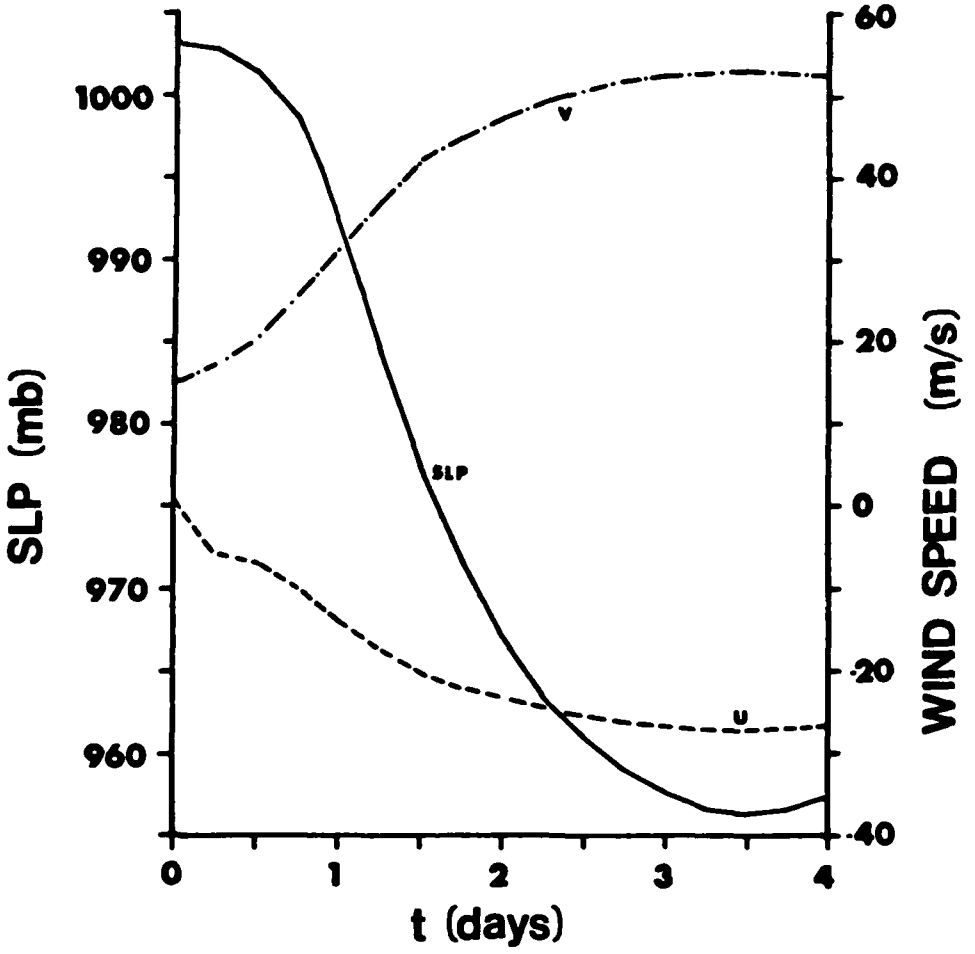

Figure 4 Minimum surface pressure (SLP), maximum tangential and radial winds with time.

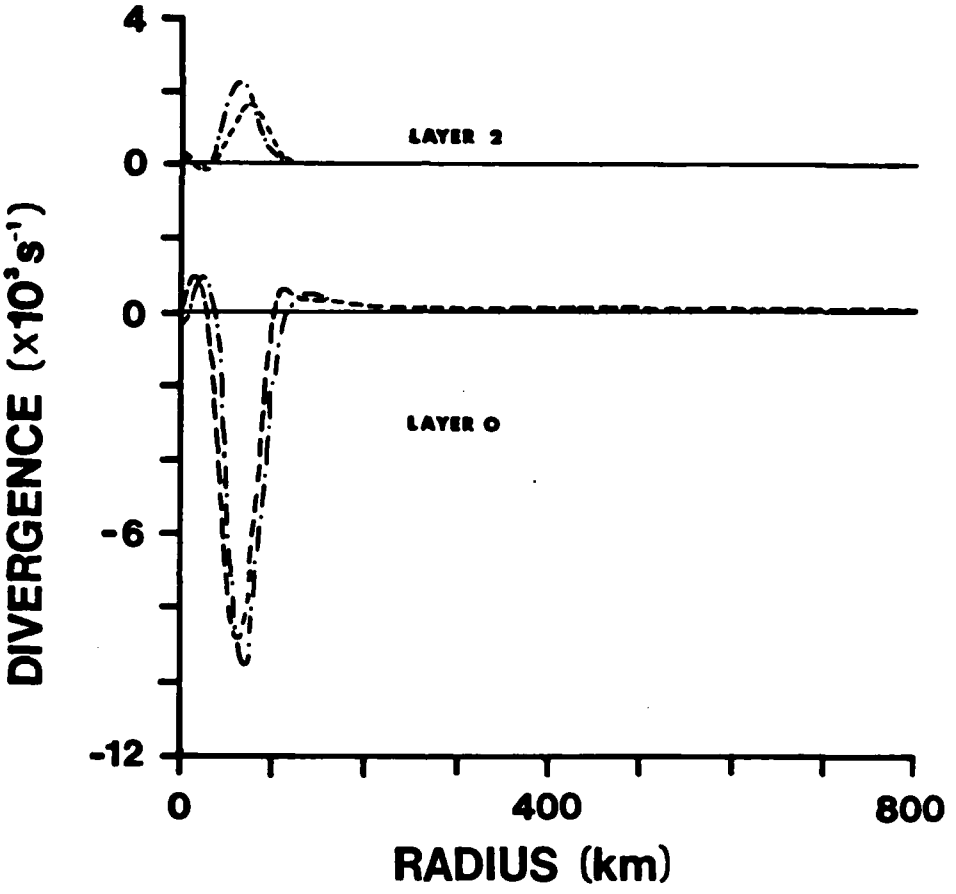

Figure 5 Profiles of divergence in layers 0 and 2 at t = 0 (solid), 48 (dash), and 96 (dash-dot) hours.

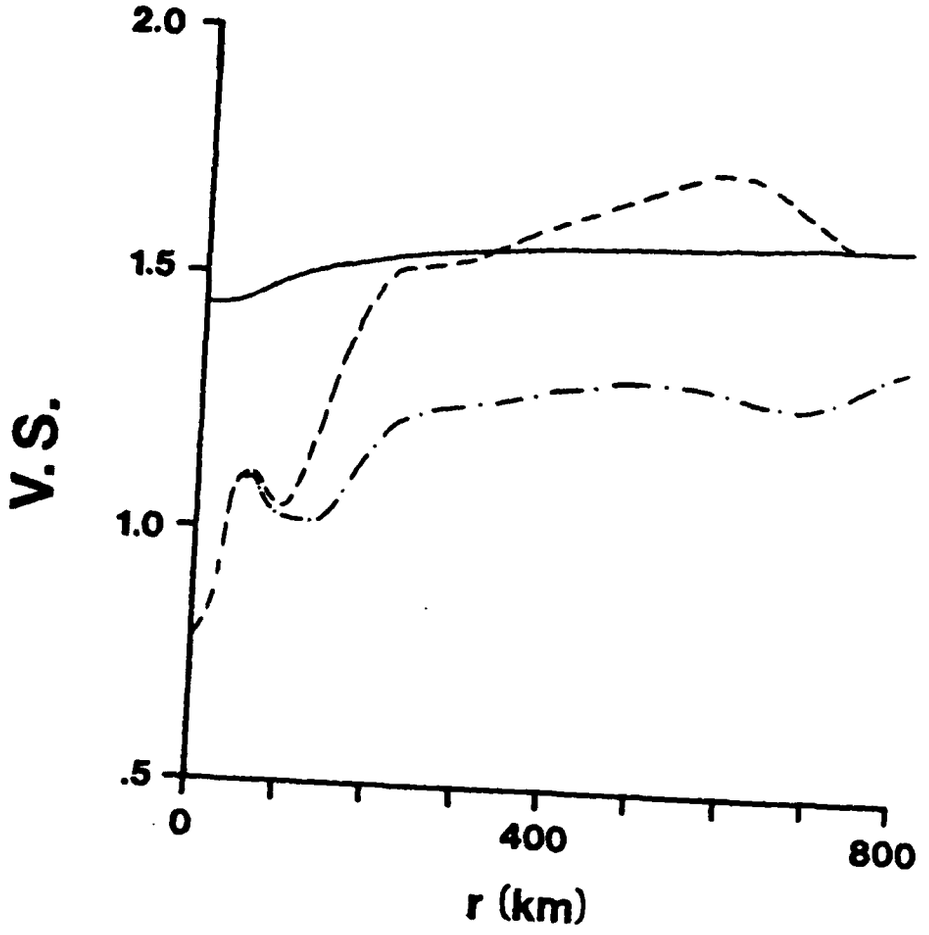

Figure 6 Profiles of the vertical stability parameter at t = 0 (solid), 48 (dash), and 96 (dash-dot) hours.

km are a result of increased evaporation as the dry, subsiding air at r = 100 km moves laterally toward the storm center. The overall gradual decrease of η in the central region of the storm is caused by the formation of the warm core, which increases $S_2^*-S_1$ with time. The outer regions of the storm show decreasing η values with time caused by large scale subsidence resulting from low-level divergence, which tends to reduce the moisture in the boundary layer.

The radii of maximum radial and tangential winds increase for the first 12 hours, then gradual decrease until day 2.5, followed by slow expansion until the end of the simulation (figs. 7 & 8). The radii of 30- and 50-knot winds were used by Weatherford (1985) to describe the aerial size of storms. In metric units, these represent the radii of 15 and 25 m/s winds, respectively. The radii of 30- and 50-knot winds in layers 0 and 1 rapidly increase during the first hours after the storm attains winds of 30- and 50-knot winds (fig. 10). Following the rapid expansion, the size of the storm increases by steady, near-linear growth. The radius of 30-knot winds increases faster than the radius of 50-knot winds.

The basic state temperature profile used in the previous simulation represented a conditionally unstable atmosphere and the boundary layer was fairly moist initially (relative humidity = 82%). Since a hurricane is

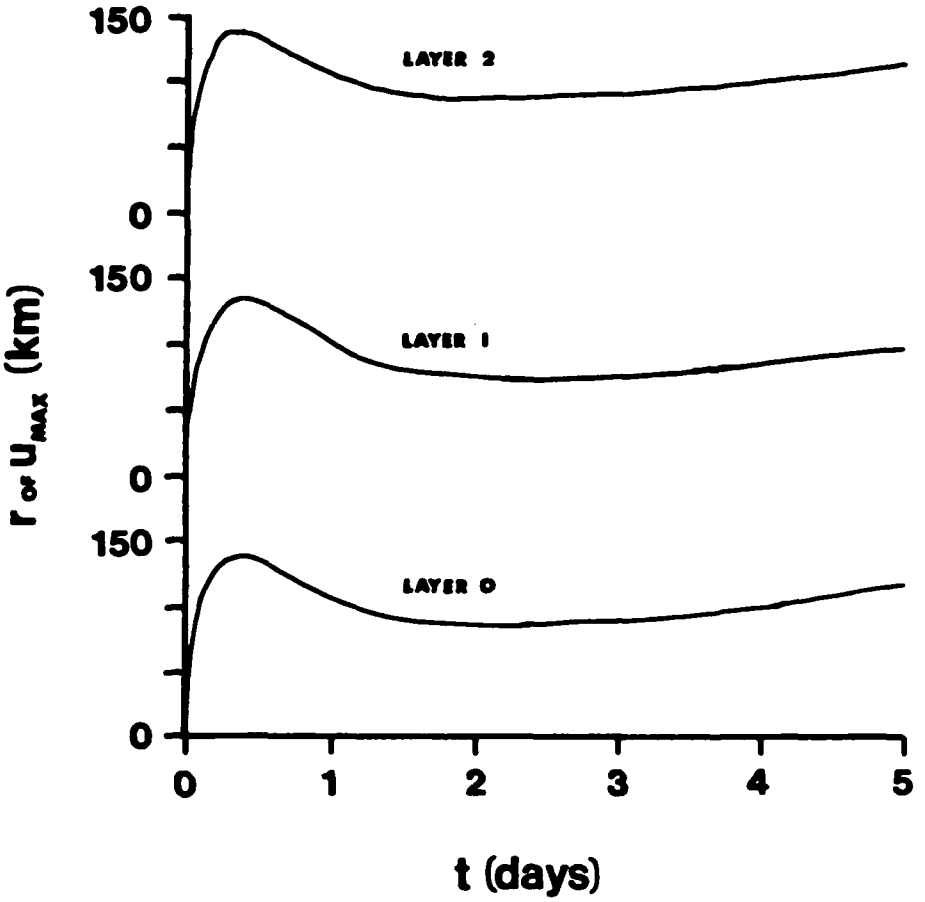

Figure 7 Radii of maximum radial winds in layers 0, 1, and 2 with time.

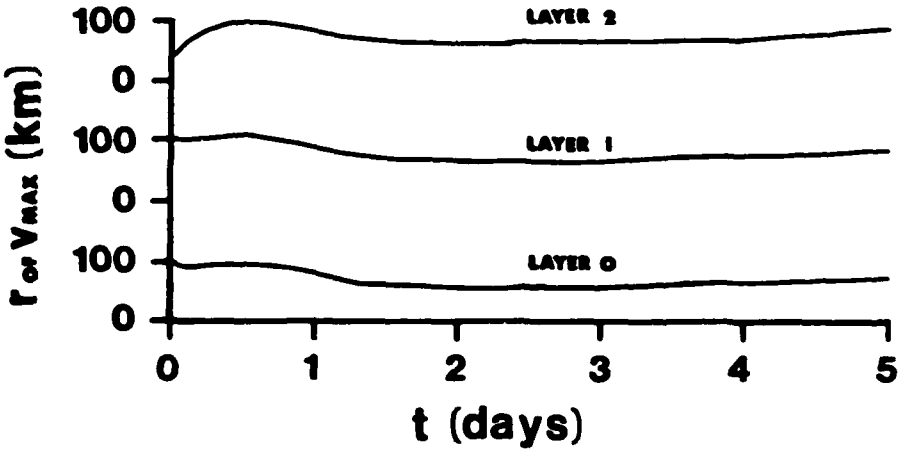

Figure 8 Radii of maximum tangential winds in layers 0, 1, and 2 with time.

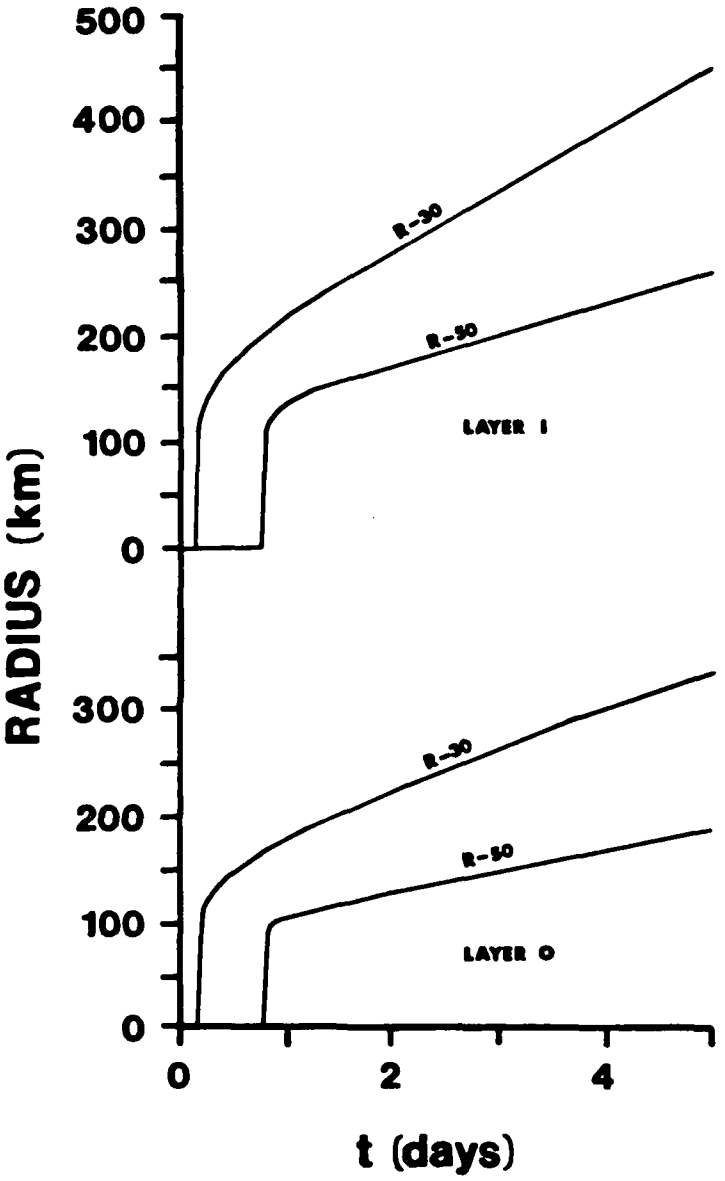

Figure 9 Radii of 30- and 50-knot winds (R-30 and R-50) in layers 0 and 1 with time.

a fairly rare event, a tropical cyclone model should be able to simulate nondevelopment as well as development (Emanuel, 1986). To test this case, the basic state potential temperature structure was changed to represent an atmosphere which was exactly moist adiabatic (θ_0 = 300°K, θ_1 = 316°K, and θ_2^* = 350°K), and the initial boundary layer moisture was reduced to q_0 = 16 gm/kg (relative humidity = 67%).

Simulations with maximum tangential wind speeds of 5 m/s produced no intensification in 5 days, whereas initial conditions with winds of 15 m/s produced a strong tropical storm. The 15 m/s case was still intensifying after 5 days of simulation, and reached a maximum intensity of 991 mb in 6 1/2 days. Using the conditionally unstable temperature and moisture profile, the 5 m/s case intensified to 1008 mb. These results are qualitatively similar to Rotunno and Emanuel's (1987) simulations which used an axisymmetric nonhydrostatic numerical model which explicitly resolved the cumulus convection.

3.2 Comparison of Cumulus Parameterization Schemes

The major difference between the study model and Ooyama's model (1969) is the cumulus parameterization scheme. Both schemes involve the calculation of the vertical stability factor, η . Ooyama assumed c_pT/θ is approximately constant so S_0, S_1, and S_2^* in the definition of η can be replaced by θ_{e0} , θ_{e1}, and θ_{e2}^* respectively.

Then θ_{eo} is predicted using a conservation equation similar to that used to calculate $\partial q_0/\partial t$, θ_{e1} is assumed constant, and θ_{e2}^* is diagnosed from the thickness of layer 2 using an analogy with a compressible fluid and an empirical relation between upper level θ_{e2}^* changes and mid-level changes. The parameterization scheme in this study allowed for more specific control of measurable parameters in the calculation of η, such as sea surface temperature and moisture content of the layers.

Keeping the initial conditions similar (table 2), the two cumulus parameterizations were compared. The results from each parameterization scheme were qualitatively similar. The major differences were that simulations using Ooyama's parameterization intensified faster than (reaching maximum intensity almost two days before) but not to the extent of (14 mb less) the study model (fig. 10). In addition, Ooyama's model produced a slightly larger storm, based on the radius of 30-knot surface winds (R-30).

3.3 Sensitivity Studies

The effects of individual parameters in tropical cyclone development were studied by systematically varying one parameter during model runs while keeping all other parameters constant. Parameters that were varied are sea surface temperature, mid-level moisture, and latitude of the storm. The sea surface temperature ranged from 24° to 30°C, mid-level moisture from 2 to 10 gm/kg (relative

Table 2: Vertical equivalent potential temperature profiles used in testing of Ooyama's (1969) model and the study model.

θ_{e2}^*	342^oK
θ_{e1}	332^oK
θ_{e0}^*	372^oK
θ_{e0}	359^oK

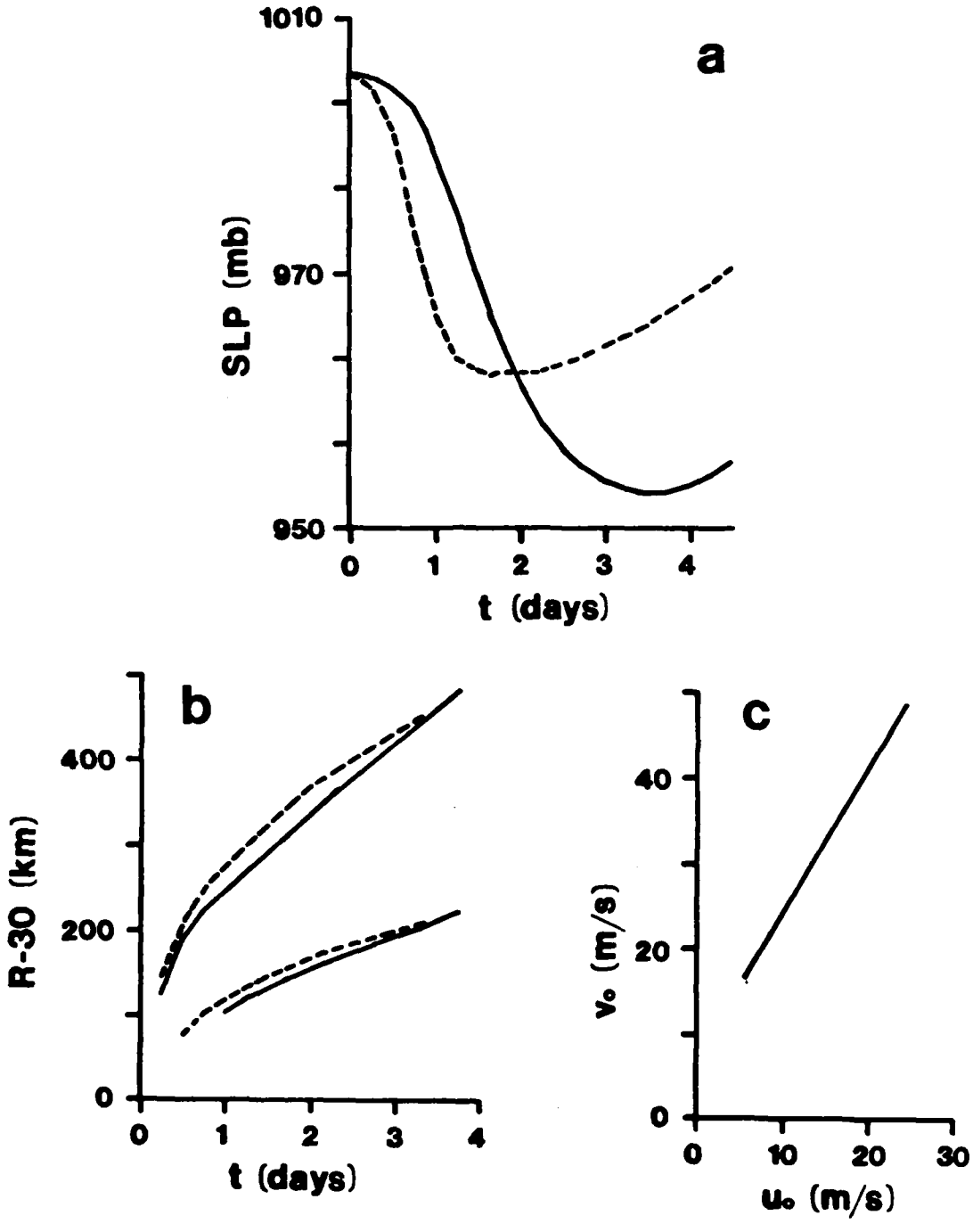

Figure 10 Comparison of results from the study numerical model (solid) and Ooyama's (1969) numerical model (dashed): (a) minimum surface pressure (SLP) with time, (b) radius of 30- and 50-knot surface winds (R-30 & R-50) with time, and (c) maximum radial versus tangential winds (both model results are identical).

humidity from 16 to 82%), and latitude from 5^{o} to 40^{o}N. The effect of seasonality was studied by using latitudinal monthly average sea surface temperatures for July, September, and November in the western Pacific calculated from Crutcher and Davis (1969).

The basic characteristics used to describe the state of the tropical cyclone were the minimum surface pressure, rate of intensification (hourly difference of the central surface pressure), maximum wind speed, radius of maximum wind speed, and outer radius of 30-knot and 50-knot surface winds (used as a measure of cyclone size in Weatherford, 1985). Individual model runs were compared for given time intervals from initiation and at two stages in the cyclone development: the period of minimum surface pressure (maximum intensification) and the period of maximum hourly change of the central surface pressure.

3.3.1 Effect of Sea Surface Temperature

The minimum surface pressure (maximum intensity) observed during the 5-day simulation decreases as the sea surface temperature increases (fig. 11). The effect of sea surface temperature on the maximum cyclone intensity is dominant compared to the effects of mid-level moisture and latitude. The maximum rate of intensification increases nonlinearly (fig. 12), while the time it takes the storm to reach maximum intensification from initiation decreases linearly with increasing sea surface temperature

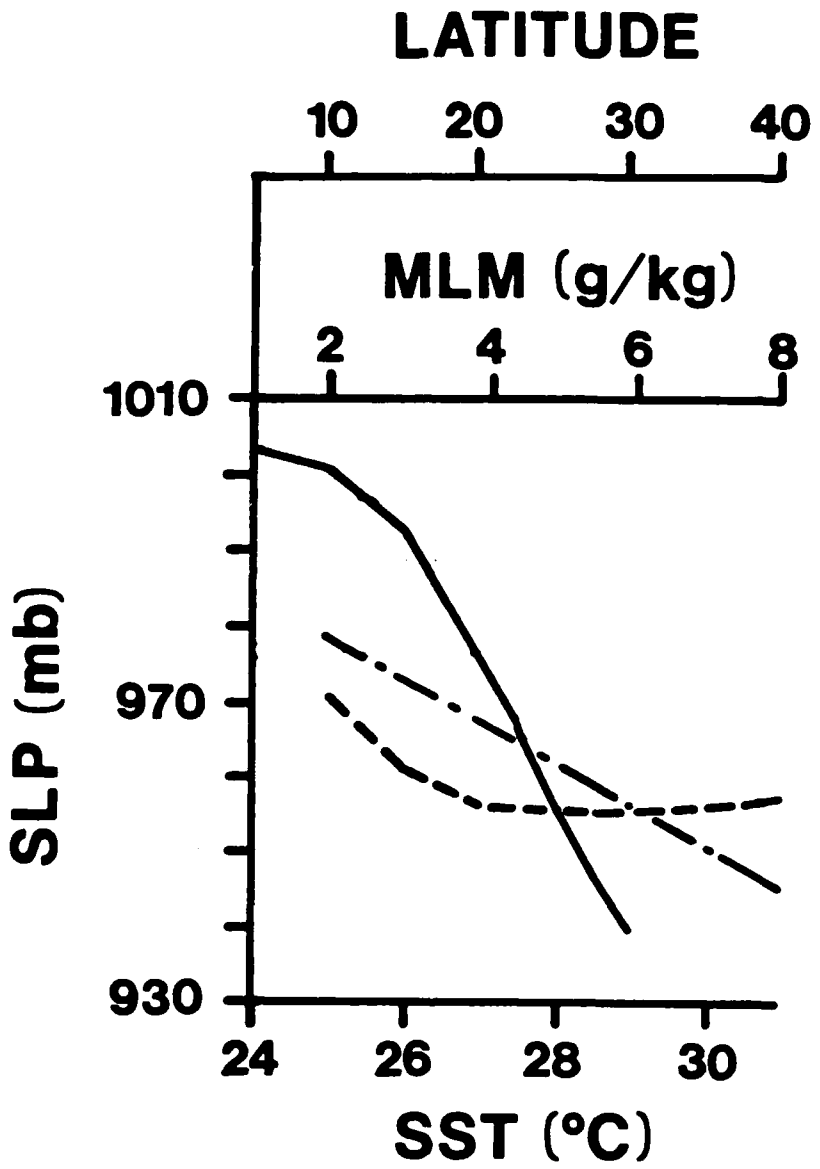

Figure 11 Minimum surface pressure (SLP) at maximum intensity with respect to sea surface temperature (solid), mid-level moisture (dash-dot), and latitude (dash).

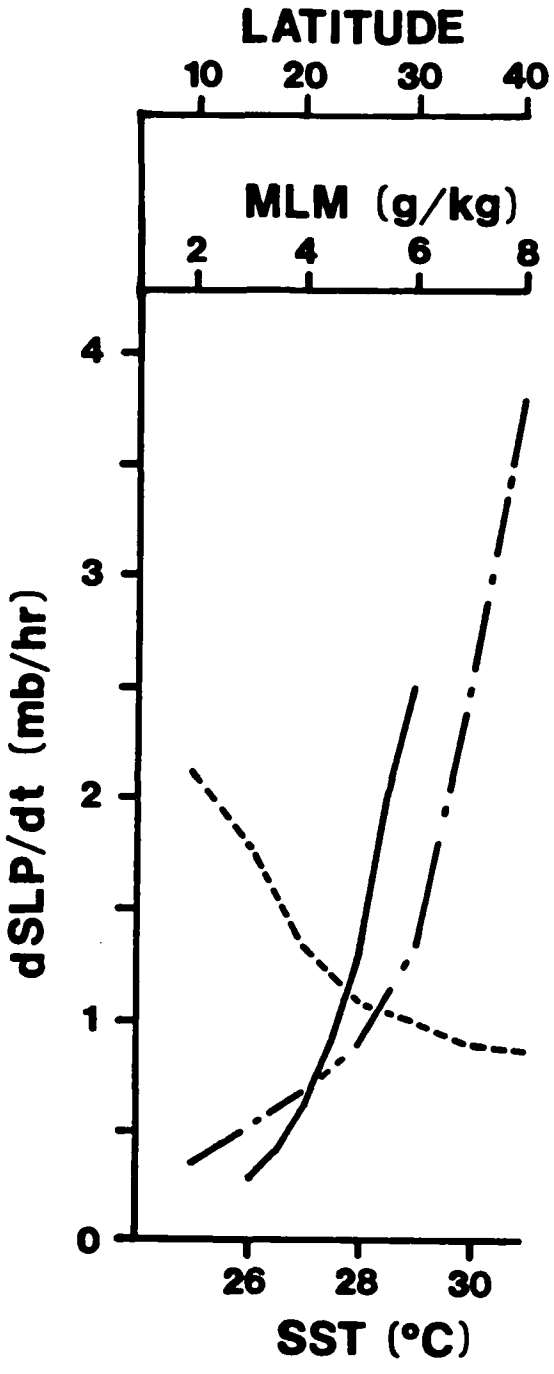

Figure 12 Maximum rate of intensification with respect to sea surface temperature (solid), mid-level moisture (dash-dot), and latitude (dash).

(fig. 13). In addition, storms that have developed over warm waters appear to deintensify more quickly than storms over cooler waters (fig. 14a).

Figure 14b shows the rate of growth in storm size. Starting from initiation, storms developing over warmer waters grow larger and more rapidly than storms developing over cooler waters. However, because the storms intensify more rapidly in warmer waters the storms are roughly the same size at the period of minimum sea surface pressure. Note that storms continue growing in size during deintensification (filling). The only case in which the size of the storm decreased during the five day simulations was when sea surface temperature was decreased during the time integration. The effects of changing sea surface temperature were estimated with this model by changing the sea surface temperature instantly for the entire storm domain. The effects of changing sea surface temperature drastically and gradually were essentially the same: the storms deintensified and decreased in size when the sea surface temperature was reduced.

3.3.2 Effect of Mid-Level Moisture

The effect of mid-level moisture is difficult to model since q_1 is held constant throughout the integration. However, it is worthwhile to determine if the model sensitivity is qualitatively reasonable. Although the mid-level moisture affects the cyclone development through

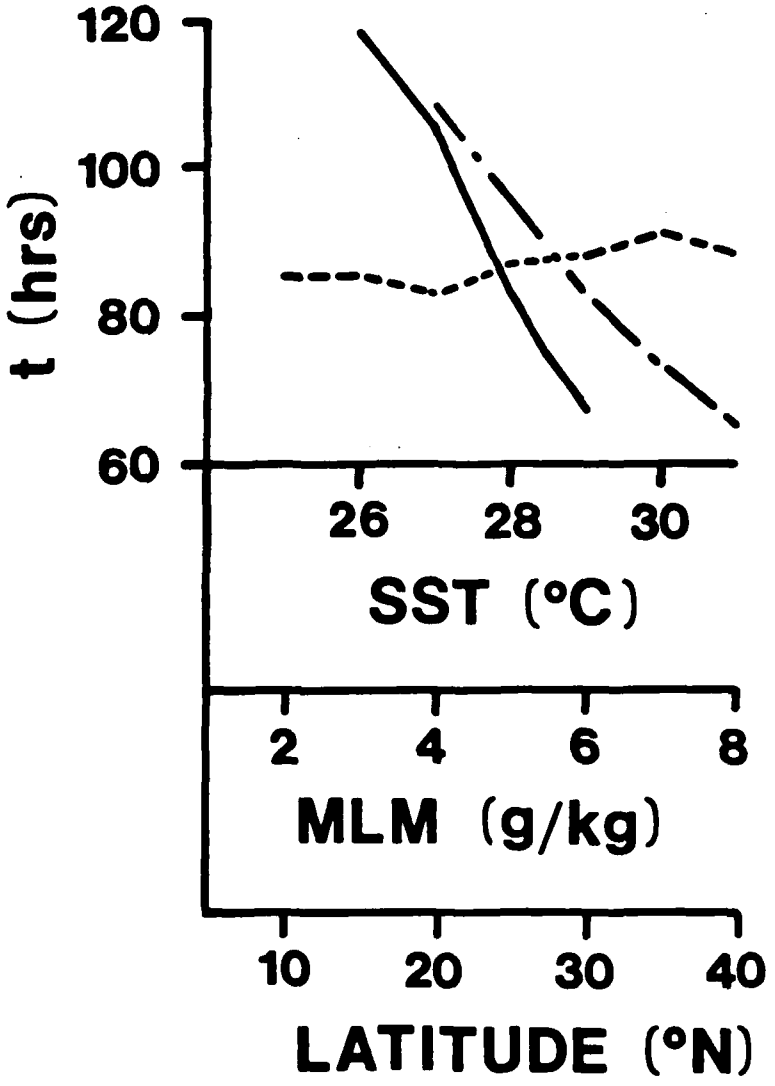

Figure 13 Time to reach maximum intensity with respect to sea surface temperature (solid), mid-level moisture (dash-dot), and latitude(dash).

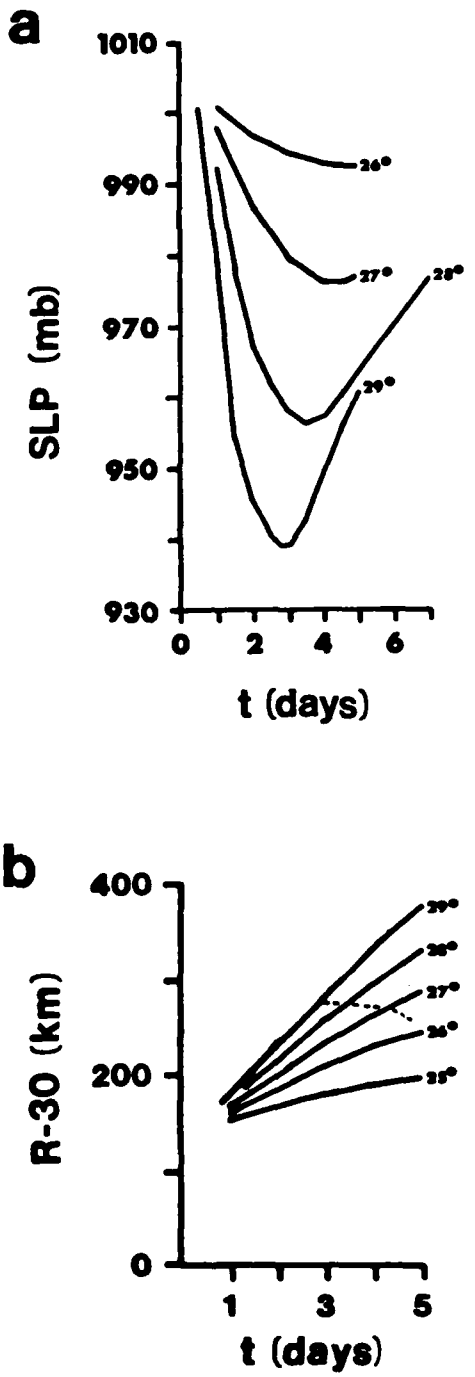

Figure 14 Effect of sea surface temperature (SST) on the (a) minimum surface pressure (SLP) with time and on the (b) radius of 30-knot winds in layer 0 (R-30) with time.

the variable, η, as does the sea surface temperature, the influence of mid-level moisture on tropical cyclone development is not identical to that caused by sea surface temperature. Figure 11 shows a linear relationship between maximum intensity and mid-level moisture whereas the sea surface temperature variations produced nonlinear variations in intensity. Although changing mid-level moisture produces smaller changes in maximum cyclone intensity, changing mid-level moisture creates large changes in the maximum rate of intensification compared to sea surface temperature (fig. 12).

In this model, mid-level moisture and sea surface temperature generally influence tropical cyclone development similarly. Storms intensify more rapidly under favorable conditions, and reach a lower minimum surface pressure. Despite growing larger and stronger more rapidly, at the time of maximum intensity the storms are roughly the same size no matter how moist the mid-levels are (fig. 15). In addition, storms with moist mid-levels deintensify faster than storms with drier mid-levels, similar to storms with a warmer sea surface temperature.

3.3.3 Effects of Latitude

Latitude affects the development of tropical cyclones through the Coriolis parameter, f, which appears in equations (45) and (46); whereas the effects of sea surface temperature and mid-level moisture are represented

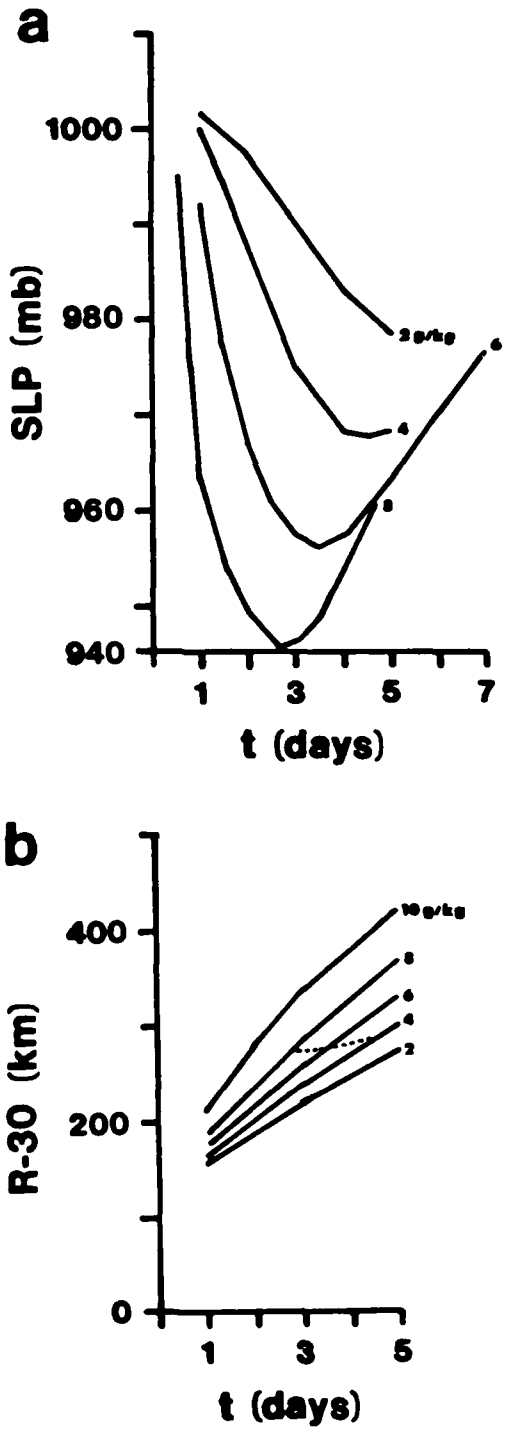

Figure 15 Effect of mid-level moisture (MLM) on the (a) minimum surface pressure (SLP) with time and on the (b) radius of 30-knot winds in layer 0 (R-30) with time.

through η, the vertical stability factor. In equations (45) - (47) η is included through the $Q^{+}_{1/2}$ and $Q^{+}_{3/2}$ terms.

With all other factors held constant, tropical cyclones intensify most between 20^{o} and 30^{o}N (fig. 11), although storms at lower latitudes experience greater rates of intensification than storms at higher latitudes (fig. 12). Starting from initialization, storms reach maximum intensity in roughly 3.5 days independent of latitude (fig. 13), although after 2 days, the cyclone at 10^{o}N did not intensify significantly (fig. 16). Storms at higher latitudes grow larger and faster than storms closer to the equator. In addition, storms at maximum intensity are significantly larger toward the higher latitudes (fig. 17).

In summary, as sea surface temperature and mid-level moisture increase, storms intensify more rapidly and intensify to a greater extent (fig. 18), yet the storm size is the same when at maximum intensity. As latitude increases, storms intensify less rapidly, generally intensify to a greater extent, and are larger when at maximum intensity.

3.3.4 Effects of Sea Surface Temperature and Latitude

It has been shown that sea surface temperature affects the intensity and size of tropical cyclones, but are the effects similar at different latitudes? Figures 19 - 21

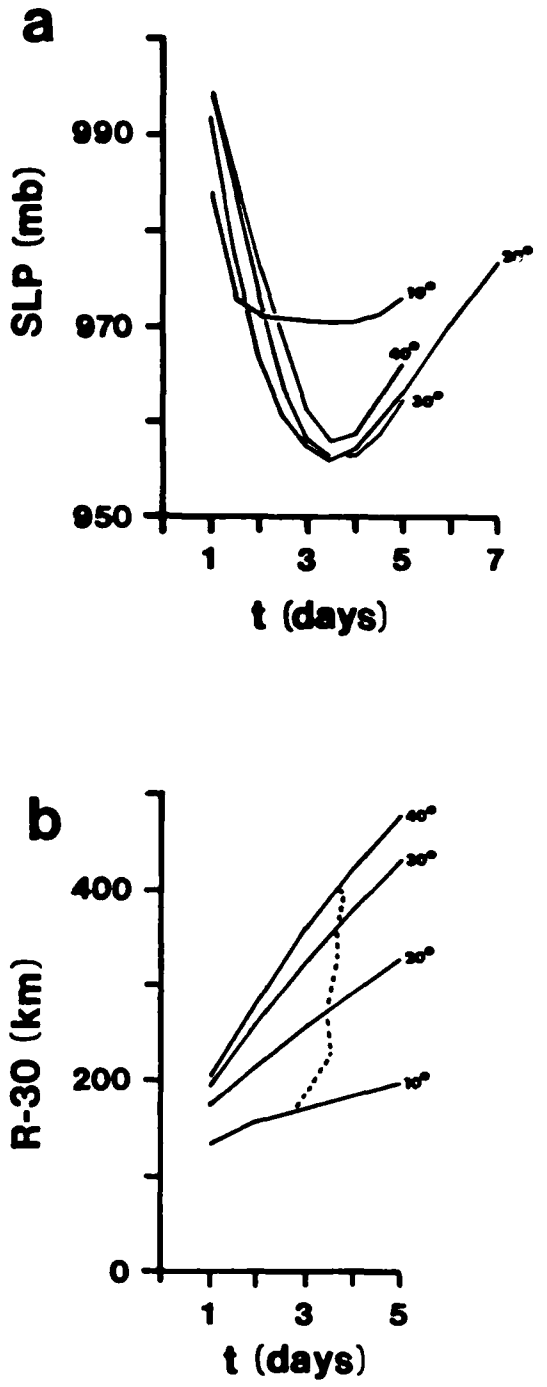

Figure 16 Effect of latitude on the (a) minimum surface pressure (SLP) with time and on the (b) radius of 30-knot winds in layer 0 (R-30) with time.

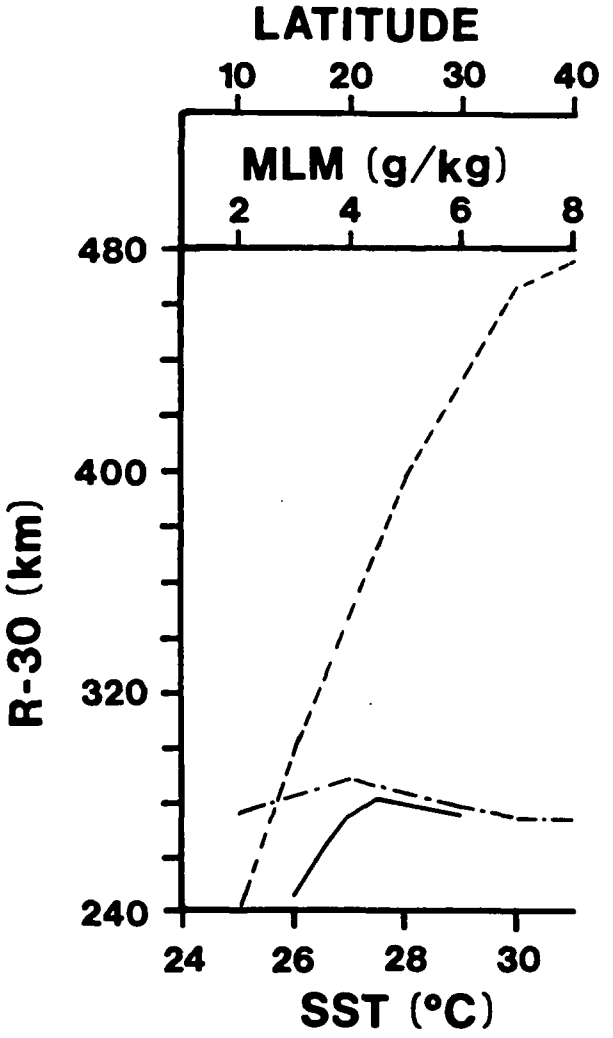

Figure 17 Radius of 30-knot winds at maximum intensity with respect to sea surface temperature (solid), mid-level moisture (dash-dot), and latitude (dash).

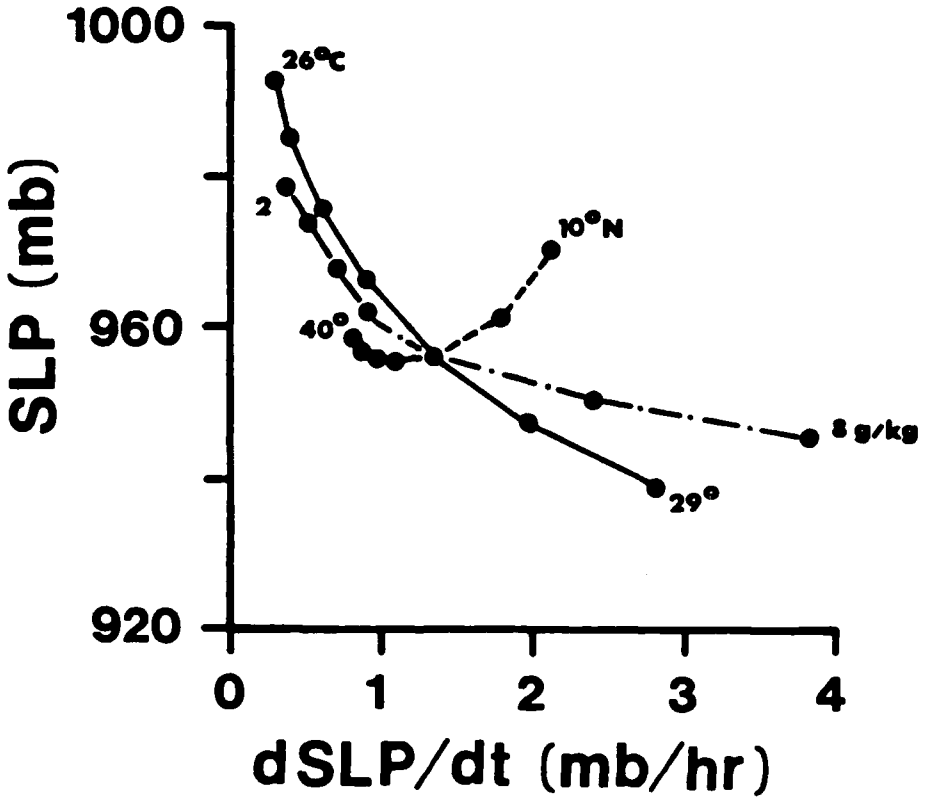

Figure 18 Effects of sea surface temperature (solid), mid-level moisture (dash-dot), and latitude (dash) on the minimum surface pressure (SLP) at maximum intensity versus the rate of maximum intensification.

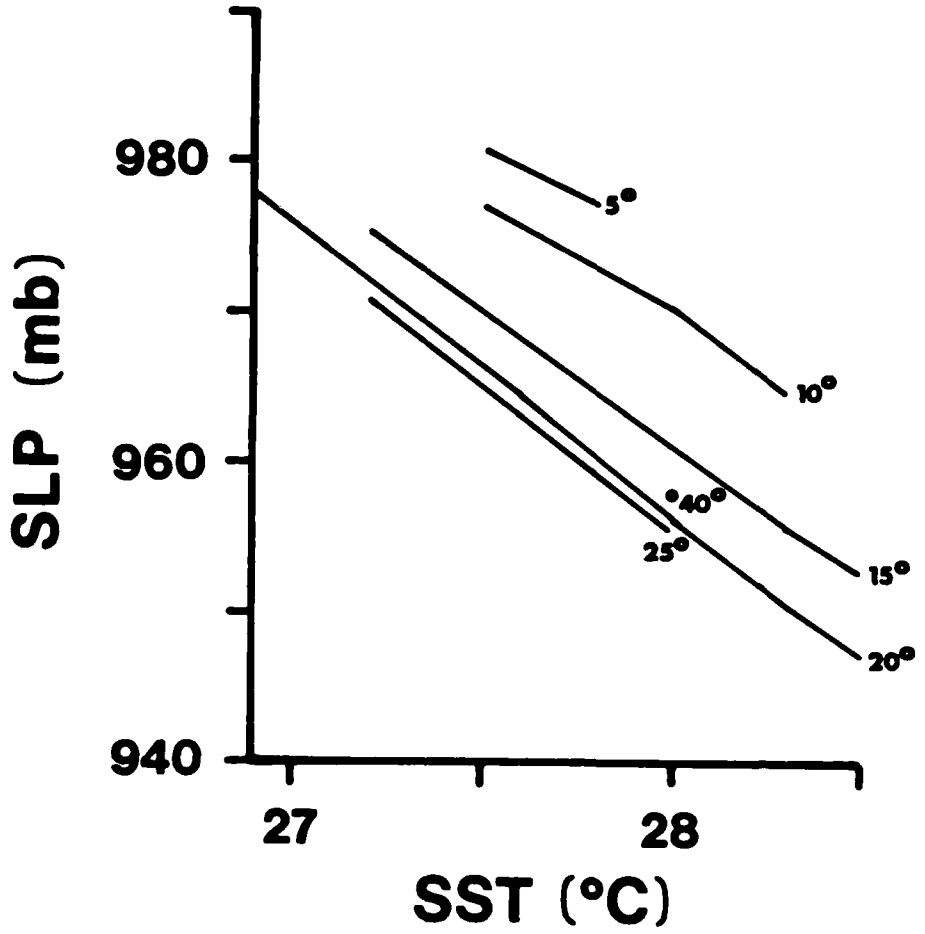

Figure 19 Comparisons of trends between sea surface temperature (SST) and minimum surface pressure (SLP) at maximum intensity for different latitudes.

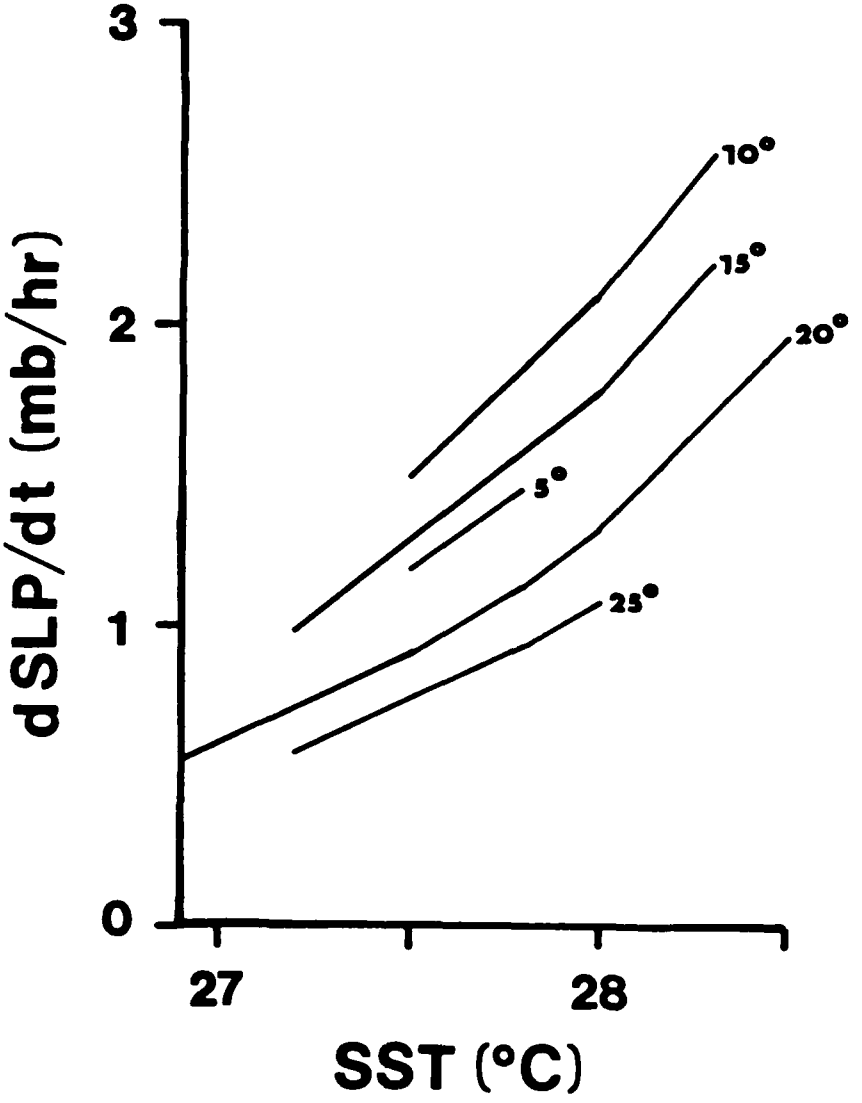

Figure 20 Comparisons of trends between sea surface temperature (SST) and the rates of maximum intensification at different latitudes.

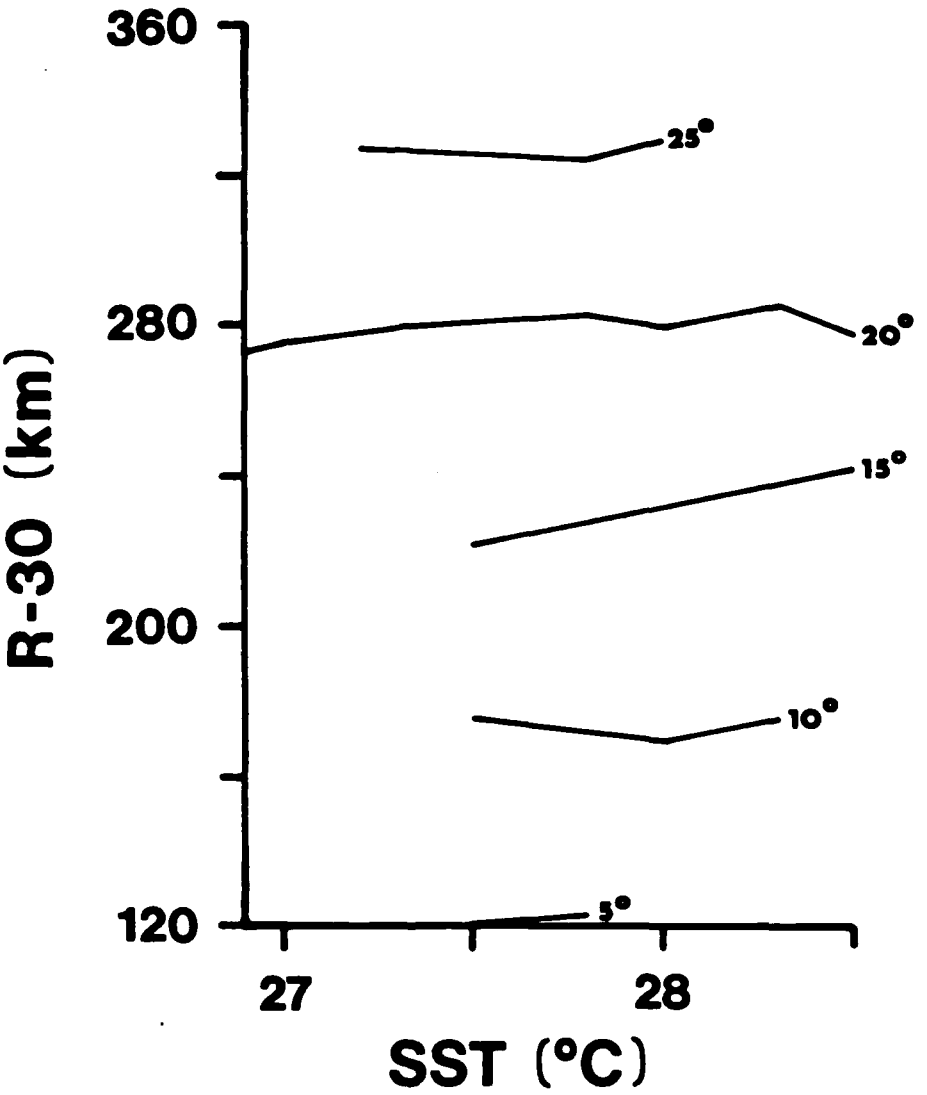

Figure 21 Comparisons of trends between sea surface temperature (SST) and radius of 30-knot winds at maximum intensity (R-30) at different latitudes.

show the effects of sea surface temperature on storms at different latitudes. Sea surface temperature influences the maximum intensity attained, the maximum rate of intensification, and storm size similarly at different latitudes, yet the magnitude of the effects vary with latitude. The nonlinear effect of latitude on tropical cyclone development is particularly noticeable when considering maximum intensity and maximum rate of intensification attained by the numerical simulations (figs. 19 & 20). In the case of maximum intensity, storms appear to become strongest between 20° and 30°N for a given sea surface temperature. Storms generally display greater intensification rates equatorward, but this reaches a maximum around 10°N. At 5°N, storms do not intensify as much or as quickly. The weak storms developing at 5°N may be a result of poor resolution on the 8 km grid. Due to the effect of sea surface temperature influencing the rate of intensification, storm size at maximum intensity is generally independent of sea surface temperature and highly dependent upon the latitude (fig. 21).

3.3.5 Effect of Seasonality

The monthly-averaged sea surface temperatures for the western Pacific (fig. 22) were used to estimate the effect of seasonality on tropical cyclones. In previous sections, with the sea surface temperature held constant, the most

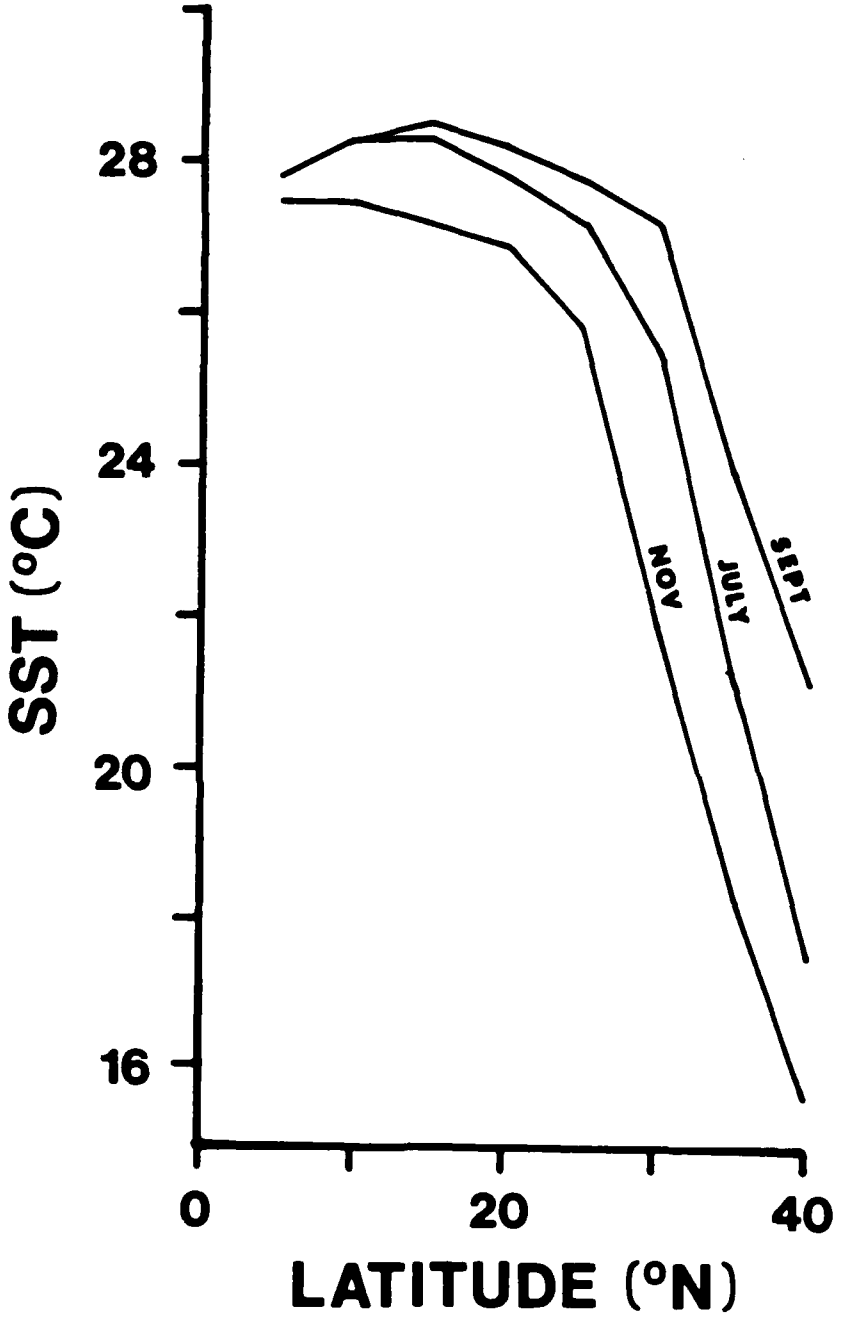

Figure 22 Latitudinal profiles of monthly-averaged sea surface temperatures (SST) (from Crutcher and Davis, 1969).

intense storms occurred between 20° and 30°N. When the latitudinal dependence of sea surface temperature is included, the most intense storms occur between 15° and 20°N in July and September, and, although much weaker, between 10° and 20°N in November (fig. 23). In addition, storms located between 10° and 15°N intensify the fastest (fig. 24). The size of the tropical cyclone at maximum intensity does not vary significantly during the season (fig. 25) as expected from the lack of influence of sea surface temperature on storm size at this stage of development.

4. COMPARISON WITH CLIMATOLOGY

4.1 Description of Data

The numerical model in this study predicts trends in the size, intensity, and rate of intensification of tropical cyclones related to sea surface temperature and latitude. Climatology data of tropical cyclones in the western Pacific were examined to see if these predicted trends in size and intensity caused by sea surface temperature and latitude are realistic. Data gathered by Air Force weather reconnaissance flights in the western Pacific from 1980 to 1982 and reduced by Weatherford (1985) was used to study the effects in latitude on tropical cyclone development. Variables that were used are:

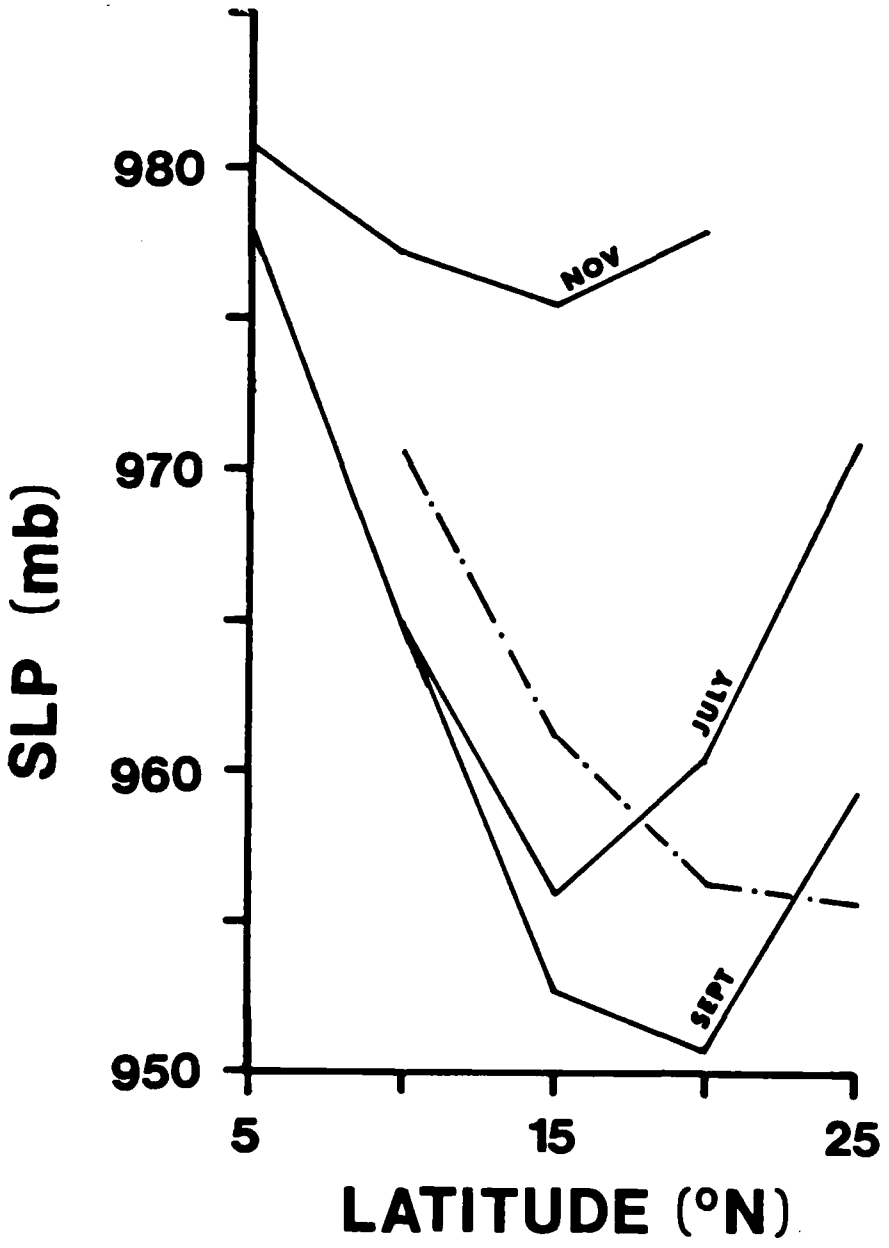

Figure 23 Seasonal changes in the minimum surface pressure (SLP) at maximum intensity with latitude. Dashed line represents model runs with sea surface temperatures of 28°C.

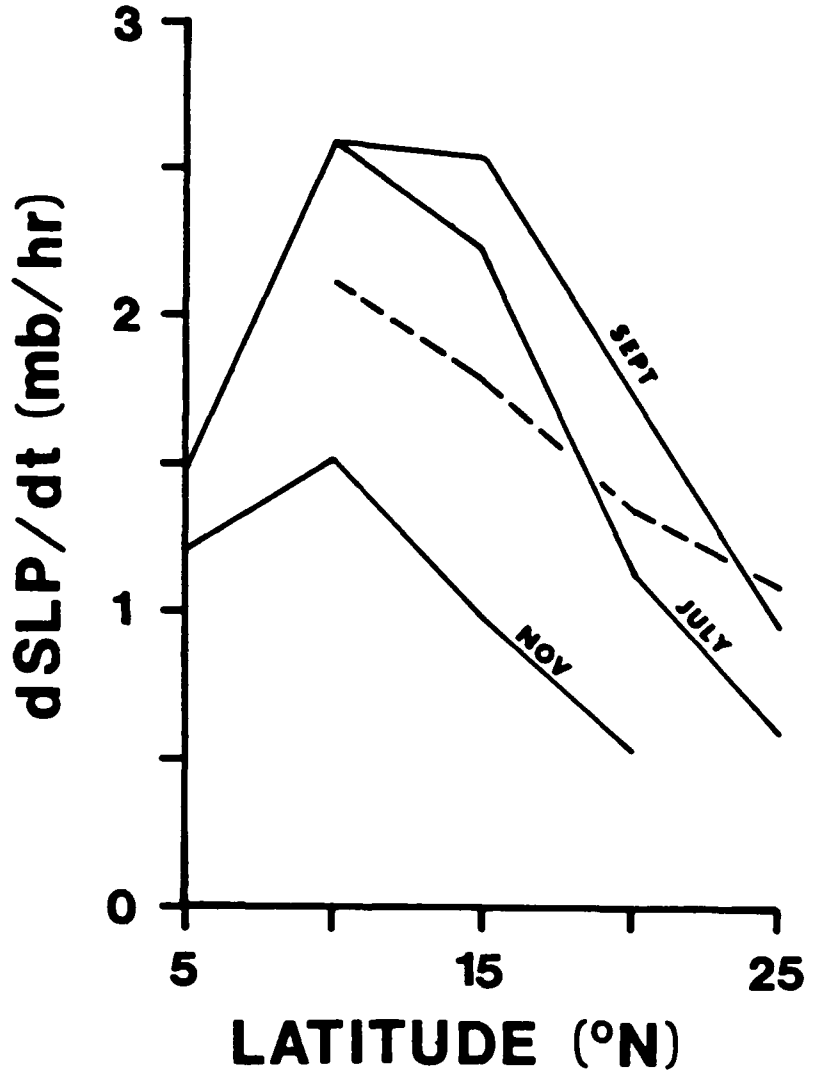

Figure 24 Seasonal changes in the rate of maximum intensification with latitude. Dashed line represents model runs with sea surface temperatures of 28°C.

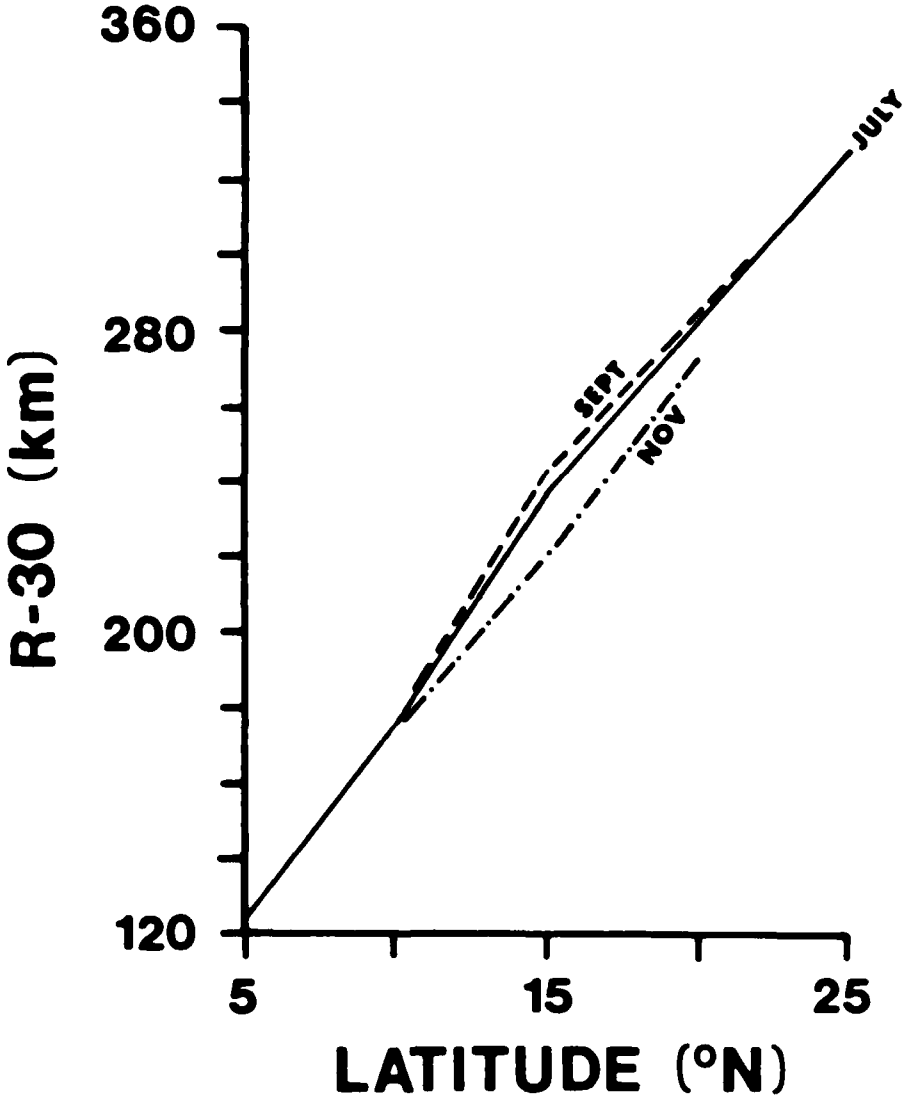

Figure 25 Seasonal changes in the radius of 30-knot winds at maximum intensity (R-30) with latitude.

R-30 : the radius (km) at which the 35-knot 700 mb wind lay on average (approximately the 30-knot wind at the surface)

LAT : latitude of cyclone center

INTL : past intensity change in meters. Difference in 700 mb minimum heights from past 12 hours to time of report

SLP : minimum observed sea level pressure.

The data were analyzed by either using all observations of storms regardless the stage of development or using data of storms at specific stages of development. Data that included multiple observations of individual storms were categorized by intervals of latitude, minimum observed sea level pressure, radius of 30-kt winds and rate of change of latitude. Using the categorized data, mean trends were compared to the numerical simulation predictions.

When the data of individual storms was complete for at least several days of observation, specific stages of development could be recognized. Two data sets were created based upon the following stages:

(1) the period of maximum change in SLP from the observations 12 hours before and after that observation, and

(2) the period of minimum SLP.

4.2 Climatology of Tropical Cyclones Regardless of Developmental Stage

When the observations of different tropical cyclones taken throughout their development were compiled, two general trends were observed: (1) storms are larger at more northerly latitudes (fig. 26), and (2) storms reach maximum intensity between 15° and 30°N (fig. 27). Figure 28 shows the effect of latitude on storms of different ranges in size and intensity. Small-, medium-, and large-size storms reached maximum intensities between 15° and 25°N. The model results for the case when sea surface temperature and latitude were varied agree with the climatological results. Without considering the effect of cooler sea surface temperature northward, the numerical model simulations reached maximum intensity between 20° and 30°N, north of the climatology results. In addition, more intense storms are larger regardless of the latitude. When the latitude and minimum surface pressure were considered (fig. 28b), storm size increased with latitude for a given intensity category, and storm size increased as intensity increased for a given latitude category.

Because numerical simulations and climatology indicate a strong dependence of latitude with the development of tropical cyclones, the influence of storm movement from one latitude to another was studied climatologically. The latitudinal movement of storms could not be realistically

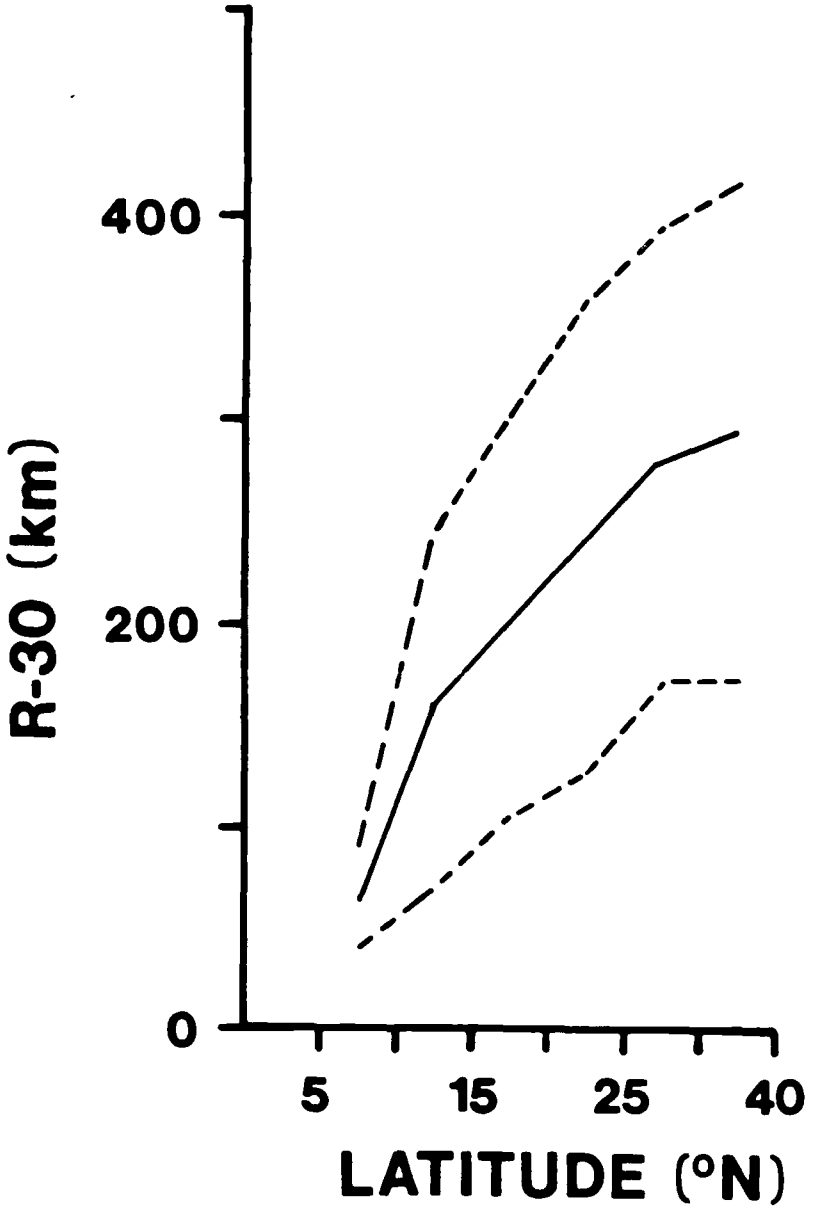

Figure 26 Climatology of the radius of 30-knot winds (R-30) with respect to latitude. The solid line represents the mean, and the dashed line represents one standard deviation from the mean.

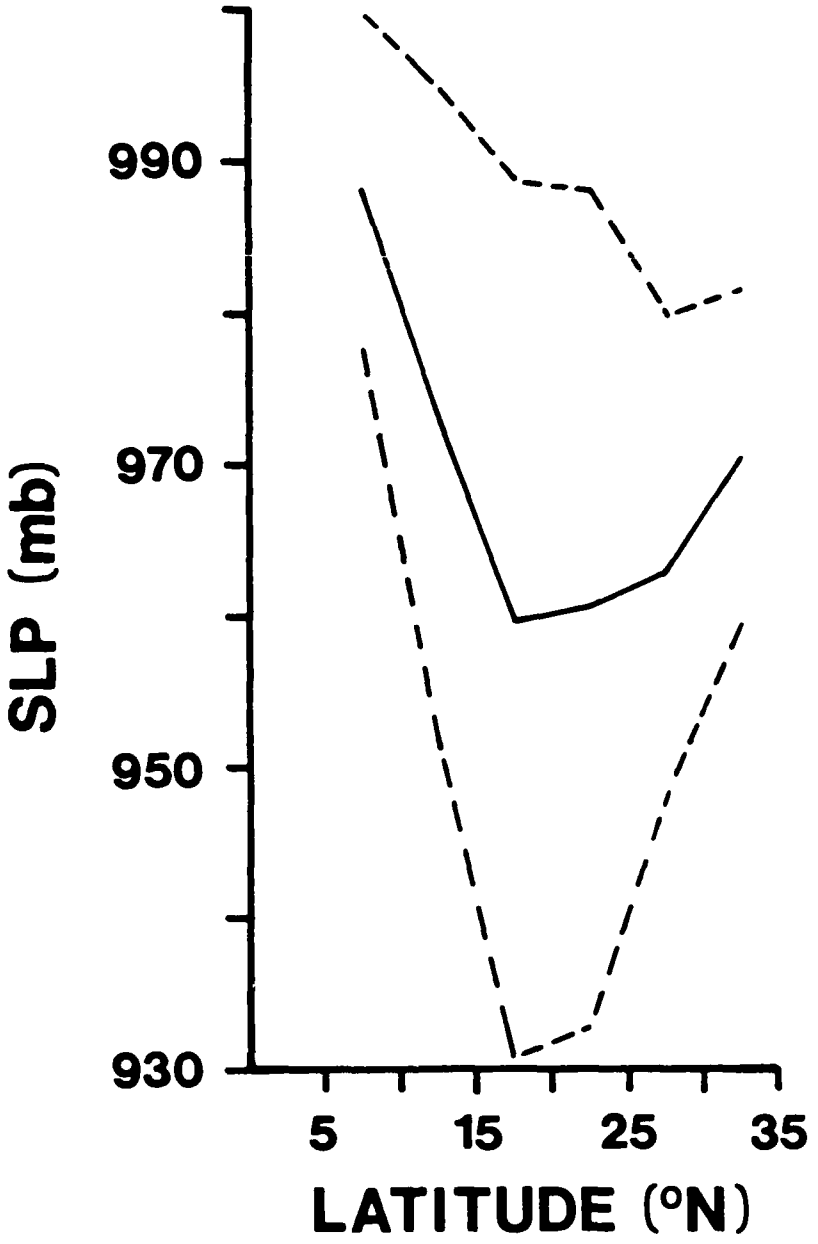

Figure 27 Climatology of the minimum surface pressure (SLP) with respect to latitude. The solid line represents the mean, and the dashed line represents one standard deviation from the mean.

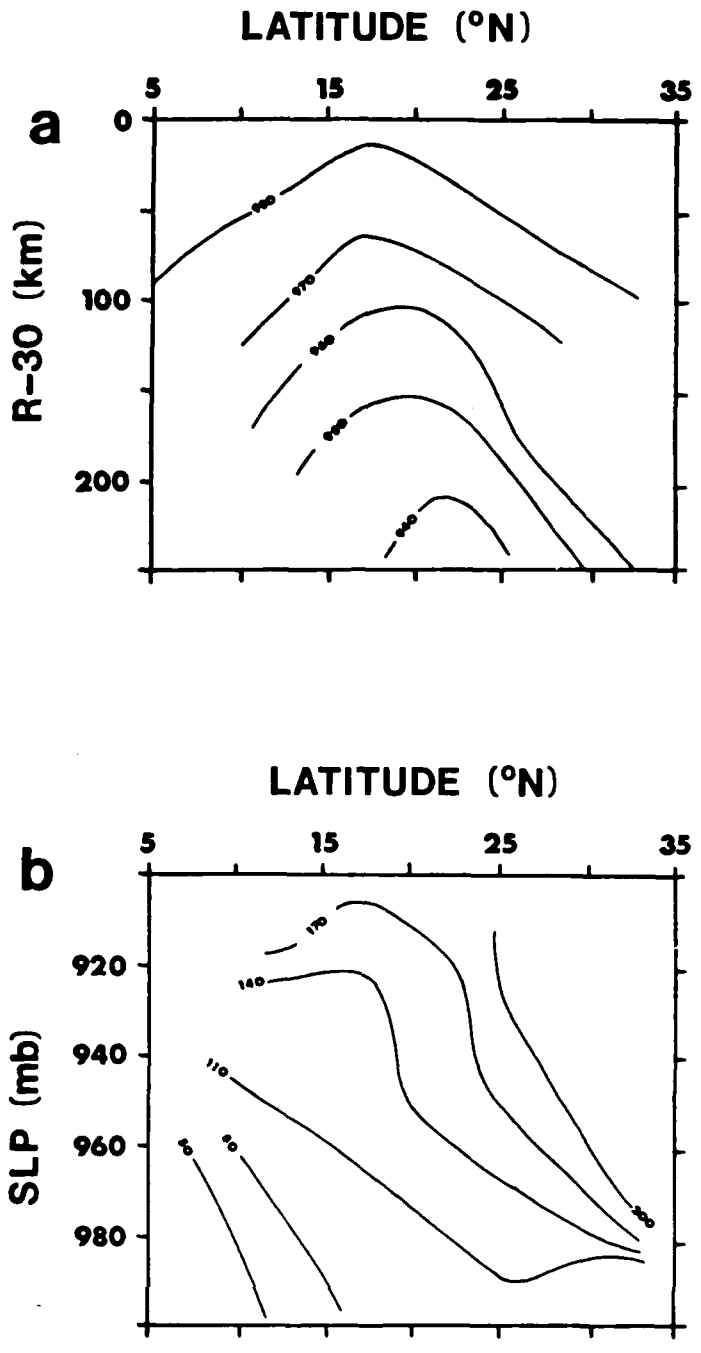

Figure 28 Climatology of (a) the minimum surface pressure (SLP) with respect to latitude and storm size (R-30) and (b) the radius of 30-knot winds (R-30) with respect to latitude and SLP.

studied using the axisymmetric model in this study. The rate of latitudinal movement was calculated in the following ways: (1) the difference between the current latitude, and the latitude at the first observation divided by time between the two observations (called the average rate of latitudinal movement) and (2) the difference between the current latitude and the latitude 12 hours previously (called current rate of latitudinal movement). The average and current rates of latitudinal movement were categorized. The effects of latitude and latitudinal movement on tropical cyclone size and intensity were studied (figs. 29 & 30). Except for storms moving southward, storms generally reached maximum intensity between 15° and 25°N regardless of the rate of poleward movement, as seen in the numerical simulations. This trend held for average rate of latitudinal movement and the current rate of latitudinal movement. In addition, the size of the tropical cyclones generally increased with latitude regardless of the rate of northward movement

4.3 Climatology of Tropical Cyclones with Respect to Developmental Stages

In order to study differences of tropical cyclones at various stages of development, the climatology data was separated into groups based on maximum rates of intensification or maximum intensity. The results are very similar to the results of the previous climatology section

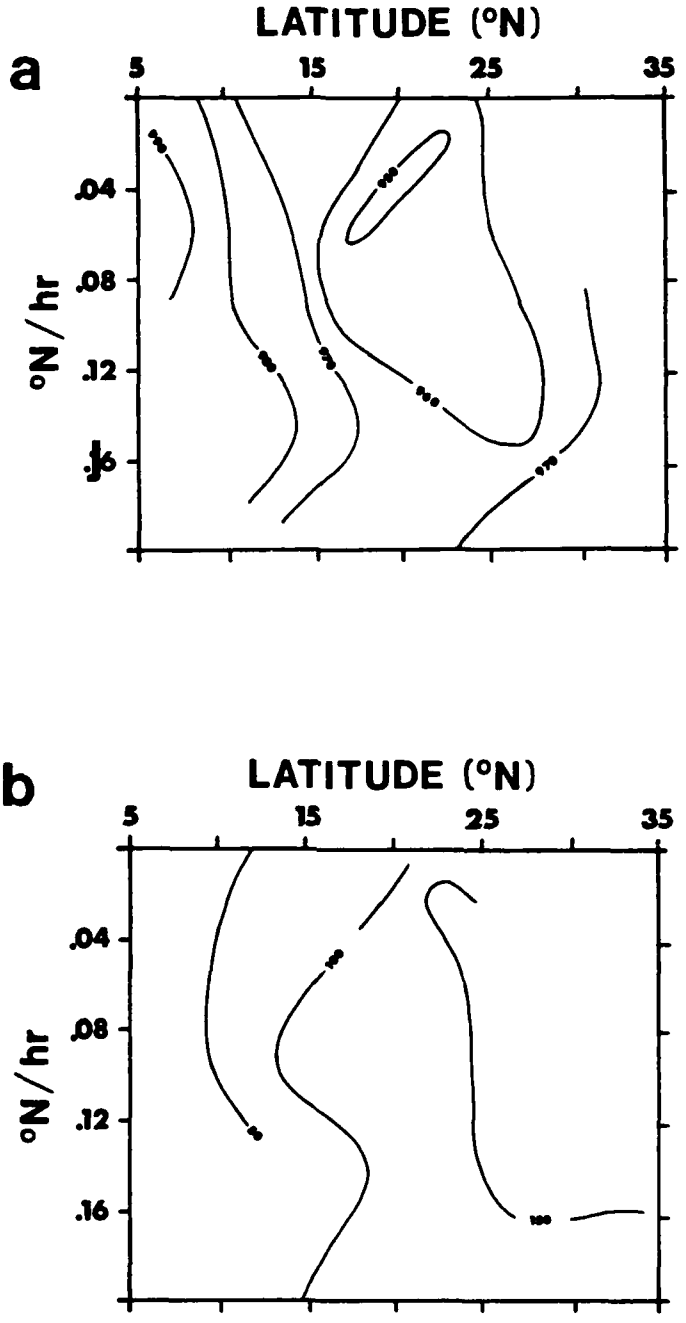

Figure 29 Climatology of (a) minimum surface pressure (SLP) and (b) radius of 30-knot surface winds (R-30) with respect to average rate of latitudinal movement and latitude.

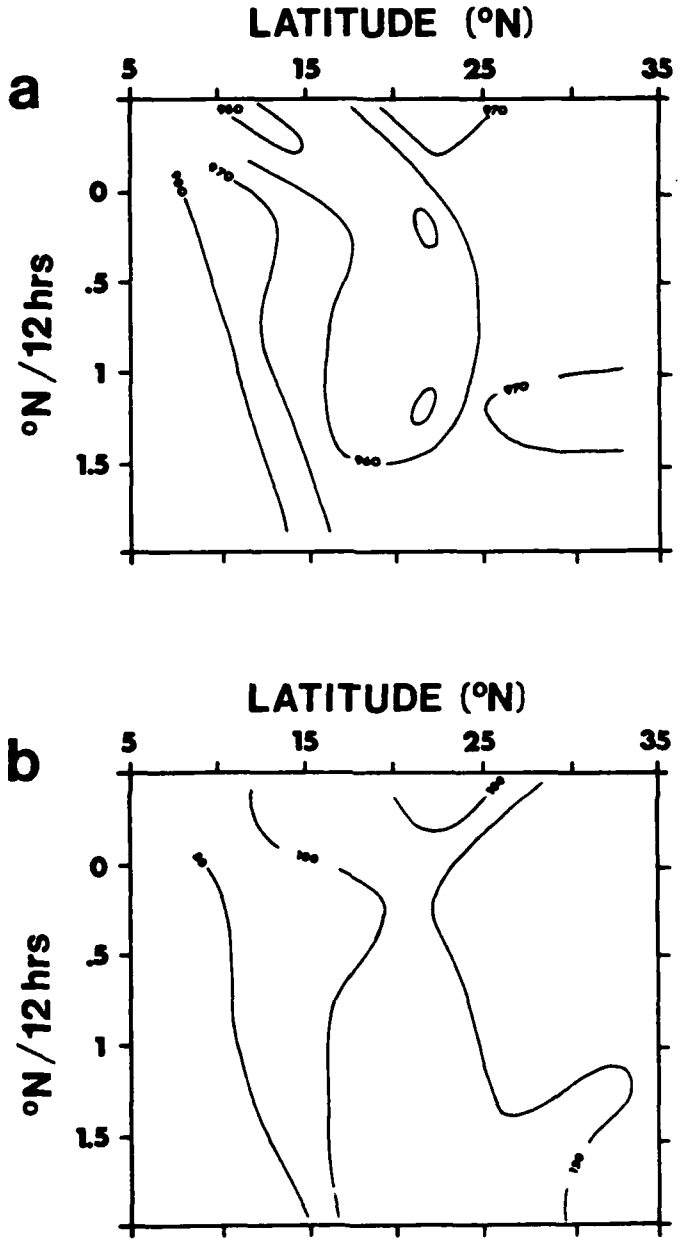

Figure 30 Climatology of (a) minimum surface pressure (SLP) and (b) radius of 30-knot surface winds (R-30) with respect to current rate of latitudinal movement and latitude.

and the numerical simulations. The most intense storms occur within 15° to 25°N (figs. 31a and 32a) and storms are generally larger poleward (figs. 31b and 32b). The decrease in size of more northerly storms is due to lack of data.

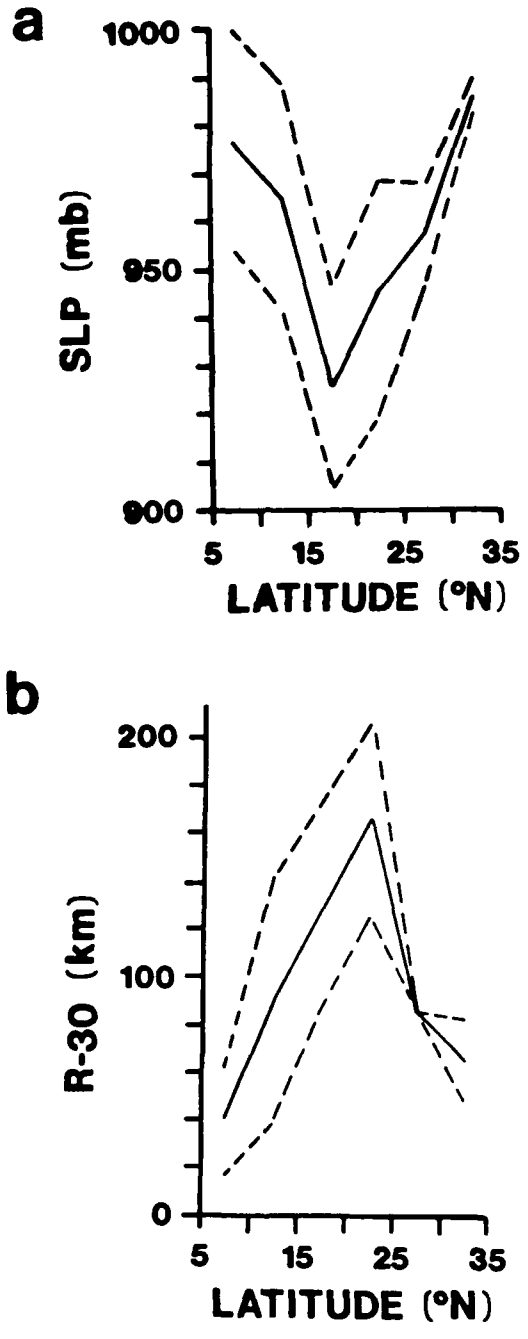

Figure 31 Climatology of the minimum surface pressure (SLP) at (a) maximum intensity and at (b) maximum rate of surface pressure change with respect to latitude. Storms are at the stage of maximum intensity. The solid line represents the mean, and the dashed line represents one standard deviation from the mean.

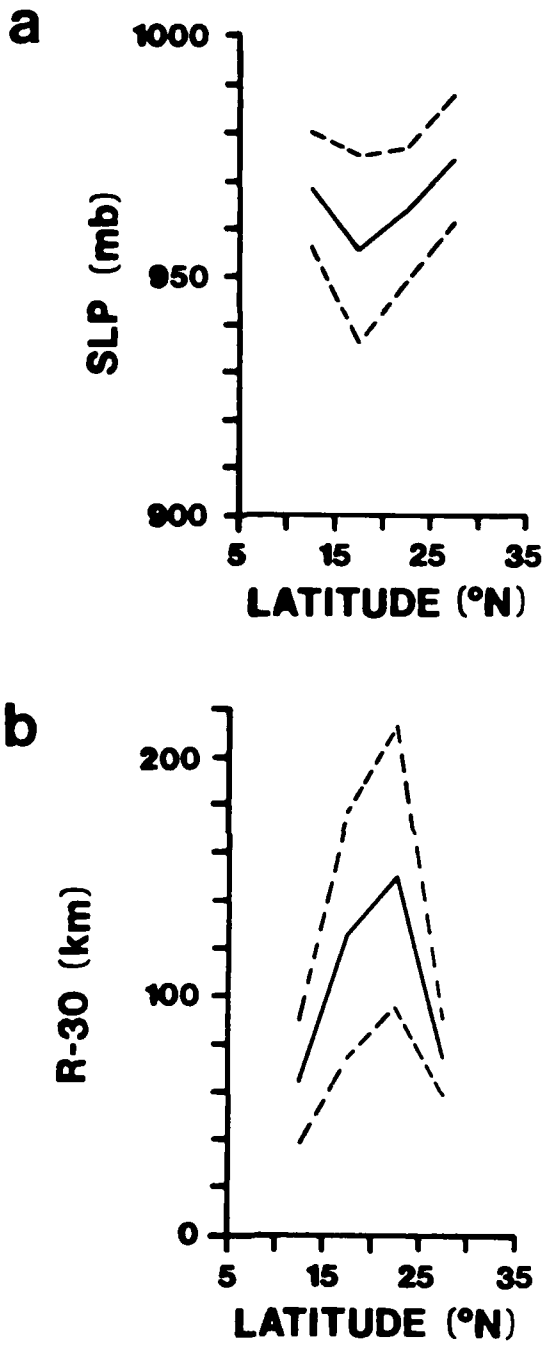

Figure 32 Climatology of the minimum surface pressure (SLP) at (a) maximum intensity and at (b) radius of 30-knot surface winds (R-30) with respect to latitude. Storms are at the stage of maximum intensification. The solid line represents the mean, and the dashed line represents one standard deviation from the mean.

5. DISCUSSION AND SUMMARY

Ooyama's incompressible fluid layer model can be rederived using isentropic layers. This makes the incorporation of thermodynamics more straight forward. In addition, the spectral method used to numerically solve the governing equations allowed simple calculation of the nonlinear terms.

The effects of sea surface temperature and mid-level moisture on the development of tropical cyclones characterized by this study are similar to those predicted in previous numerical modeling research (Ooyama, 1969; Sundquist, 1970; Rosenthal, 1970, 1971), and climatologically (Gray, 1968, 1979; MacBride, 1979). In both cases, the influences are monotonic: increasing storm strength, size, and rate of development with increasing sea surface temperature and/or mid-level moisture. However, storms are the same size at maximum intensity. The greater the sea surface temperature or mid-level moisture, the greater the amount of moisture available for condensation and latent heating per unit volume of ascending air. By the CISK theory described by Ooyama (1982), this increased latent heat release would produce a feedback which causes faster and greater tropical cyclone development.

Because the maximum heating is located slightly inside of the radius of maximum winds, the radius of maximum winds decreases with time as the storm intensifies (figs. 7 & 8).

Because there are greater amounts of heating occurring closer to the center of the storm, storms with moister mid-levels or over warmer oceans intensify faster and stronger than storms with drier mid-levels or cooler ocean temperatures (fig. 18). In addition, the more intense storms tend to deintensify more rapidly because the high rates of heating required to maintain such strong storms is not possible with the decreasing η values and because surface drag is nonlinear. Because heating of the mid-levels decreases the conditional instability of the temperature lapse rate, storms with rapid heating quickly lose their ability to maintain cumulus convection.

The effect of latitude is not monotonic as described in previous literature (Yamasaki, 1968). Yamasaki only studied three latitudes (0°, 4° and 20°N) to describe the effect of latitude. In this study, storms at 5°N intensify slowly and become very weak storms. Interestingly, most numerical model studies use 20°N as the typical latitude for tropical cyclones, which is within the bands of climatologically intense storms and of numerically simulated strong tropical cyclones.

When the latitudinal variation of sea surface temperature is neglected, storms within 20° - 30°N latitude intensify the most, yet do not intensify most rapidly. Storms at lower latitudes (near 10°N) are very small and relatively weak, and tend to intensify very quickly. Whereas

when sea surface temperature or mid-level moisture vary, storms that intensified most also intensified the fastest. Latitude does not directly influence the availability of moisture as sea surface temperature and mid-level moisture do, but latitude does influence the positioning of the maximum heating (fig. 33) and the relationship between u and v (fig. 34). Sea surface temperature and mid-level moisture did not affect the relationship between u and v; the trend is shown in Figure 10c.

Schubert and Hack (1982) described the effects of inertial stability on the efficiency of heating within a tropical cyclone. The greater the inertial stability for a given heating field, the greater the efficiency of heating, and, therefore, the greater the rate of intensification. Figure 35 shows that storms at low latitudes have greater inertial stability at the radius of maximum heating of the storms in addition to greater rates of heating, so these storms intensify the fastest. But because the storm is intensifying so quickly, the η profile is being modified more rapidly (fig. 36) and the environment in the region of maximum updraft and heating becomes less and less conditionally unstable, causing the storm to stop intensifying. In the case of 10^{o}N, the vertical instability, although small, is large enough to allow the storm to maintain the maximum intensity for several days (fig. 16). In addition, inertial stability is greatest at

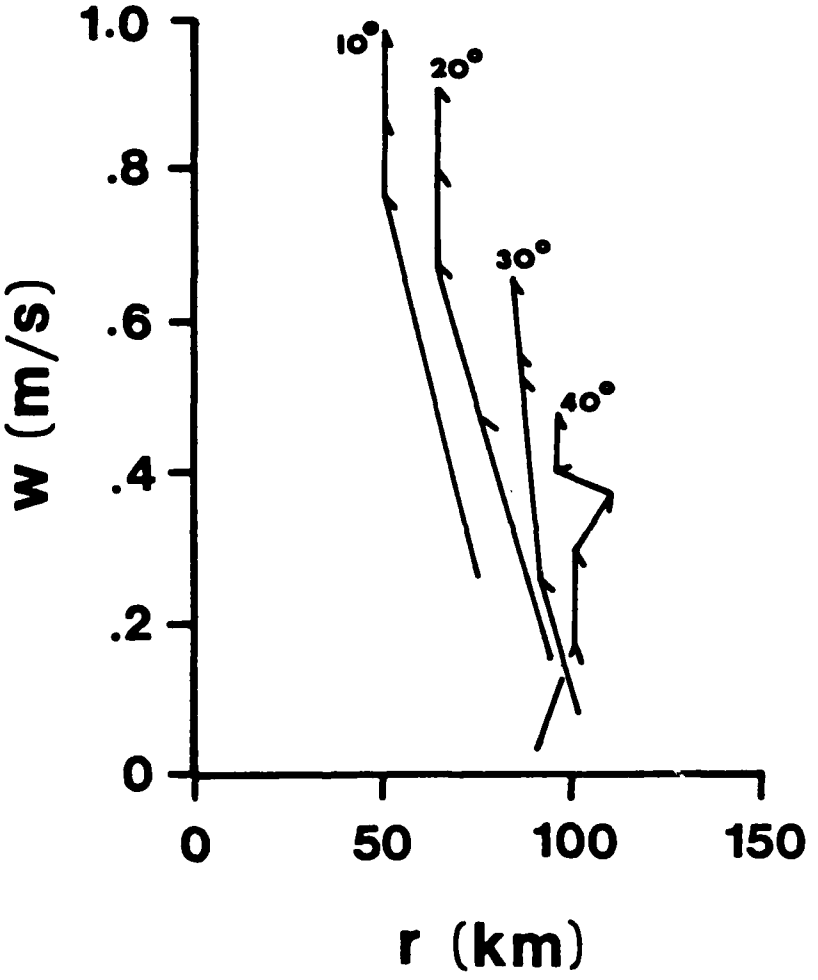

Figure 33 Radial distribution of the maximum vertical velocity with time and latitude.

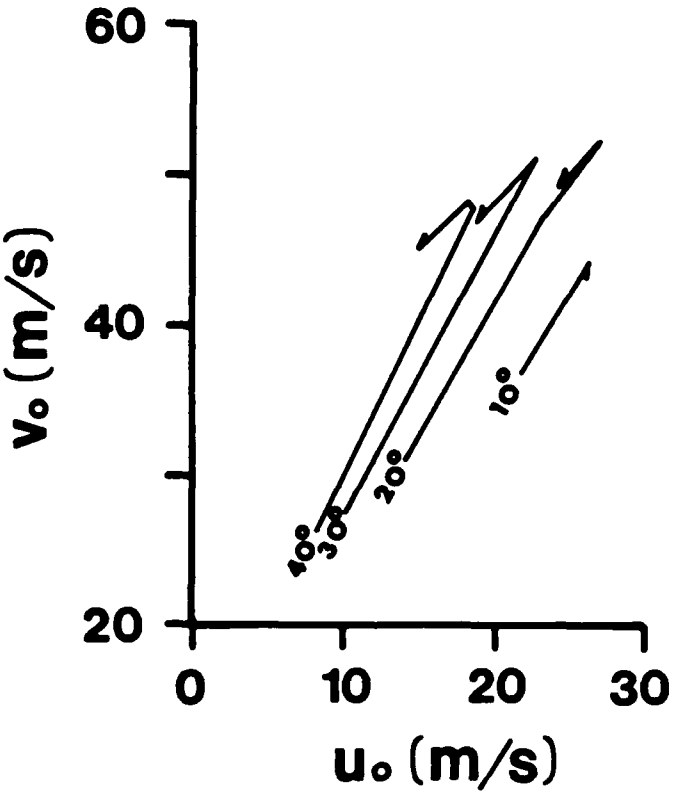

Figure 34 Maximum radial winds versus maximum tangential winds in layer 0 with respect to time and latitude.

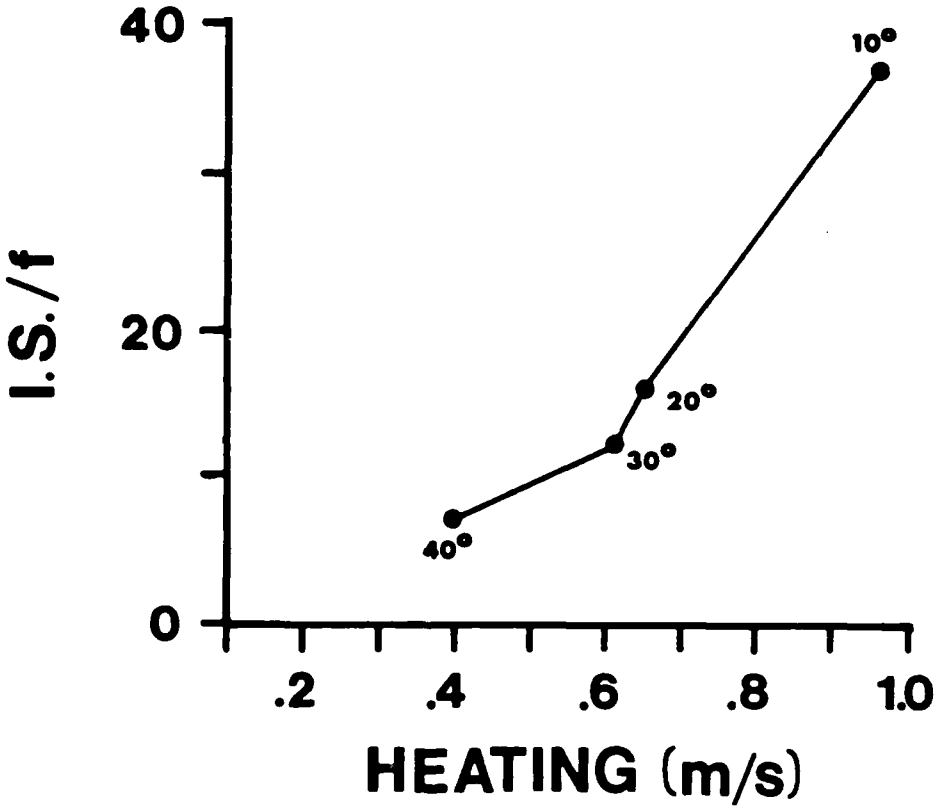

Figure 35 Inertial stability at radius of maximum heating with respect to latitude. The inertial stability values have been normalized by the corresponding Coriolis parameter, f.

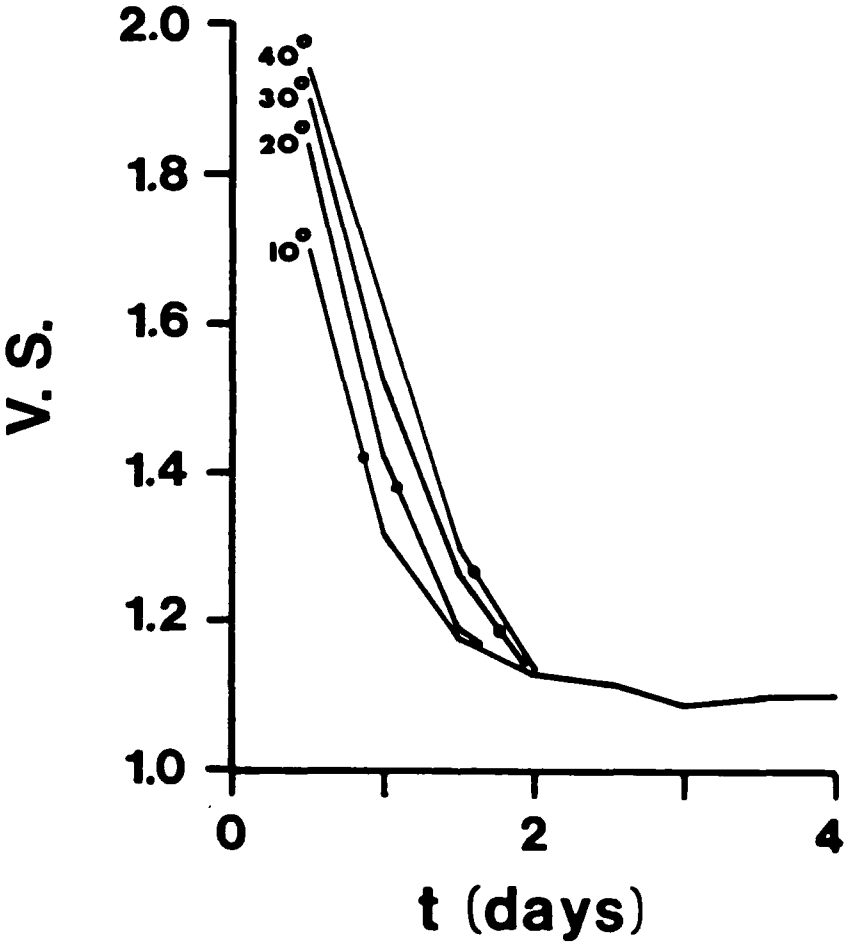

Figure 36 The vertical stat[illegible]
of maximum ver[illegible]
time and lat[illegible]de

AD-A185 670 THE EFFECT OF LATITUDE ON THE DEVELOPMENT OF TROPICAL CYCLONES(U) AIR FORCE INST OF TECH WRIGHT-PATTERSON AFB OH J D PICKLE 1987 AFIT/CI/NR-87-95T 2/2

UNCLASSIFIED F/G 4/2 NL

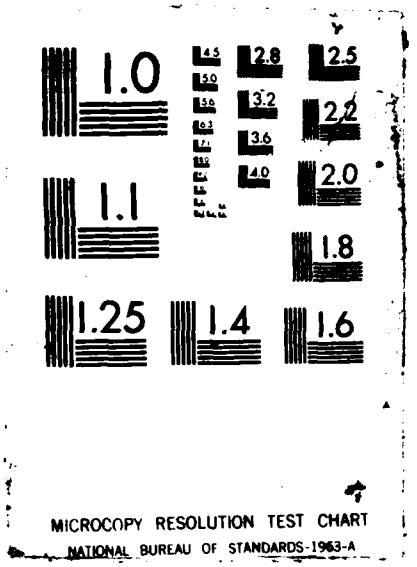
1.0
1.1
1.25
1.4
1.6
2.8
3.2
3.6
4.0
2.5
2.2
2.0
1.8
MICROCOPY RESOLUTION TEST CHART
NATIONAL BUREAU OF STANDARDS-1963-A

lower latitudes so that for even small rates of heating, the greater efficiency of heating allows the storms to maintain its maximum intensity which is small compared with storms at higher latitudes. Also, surface drag is not as great.

Tropical cyclones at higher latitudes tend to intensify at slower rates but intensify more than lower-latitude storms. A factor that will cause northerly storms to spin up more slowly is that the radius of maximum updraft and heating is farther from the center of the storm and weaker compared to storms at lower latitudes. The weaker rate of heating, results in the slower rate of spin up. By the conservation of angular momentum, if the forcing of the storm is farther from the center the response will be to produce a larger storm with slower tangential winds. Because the heating is occurring further from the center, the conditional instability takes longer to modify. So the northerly storms intensify longer but at slower rates. This allows the poleward storms to reach relatively strong maximum intensities.

When both latitudinal variation of sea surface temperature and latitude are considered, the results of the numerical simulations are very similar to the climatology results (fig. 27). Because storms at lower latitudes are over waters with relatively warm temperatures, the absence of large, strong storms is more a result of latitude. The

latitudinal band (15^{o} – 25^{o}N) where relatively strong large storms occur, is a result of latitude effect and sea surface temperatures. North of this band, the absence of strong storms is primarily a result of the sea surface temperature, yet the larger storm size (i.e., radius of 30-knot winds) is a result of latitude. In summary, storm size is affected predominately by latitude at all latitudes, and the maximum storm intensity is affected by latitude at lower latitudes, latitude and SST at 15^{o}–25^{o}N, and sea surface temperature at higher latitudes.

The effect of storms moving north from low latitudes does not seem to be climatologically related to how fast or how much a tropical storm develops. Yet from the numerical simulations, storms that are spinning up rapidly in lower latitudes would tend to intensify more as the storms move into higher latitudes. Thus, as the storm moves northward, the radius of maximum heating expands which allows the storm to intensify longer, and so stronger. Further studies of this effect should be made with a three-dimensional model.

6. LIST OF REFERENCES

Anthes, R.A., 1982: Tropical cyclones: their evolution, structure and effects. Meteorological Monographs, v. 19, No. 41, American Meteorological Society, 208 pp.

Brand, M., 1972: Very large and very small typhoons of the western north Pacific Ocean. Journal of the Meteorological Society of Japan, v. 50, p. 332-341.

Charney, J., and A. Eliassen, 1964: On the growth of the hurricane depression. Journal of the Atmospheric Sciences, v. 21, p. 68-75.

Crutcher, H.L., and O.M. Davis, 1969: U.S. Navy Marine Climatic Atlas of the World, Volume III. Naval Weather Service Command, NAVAIR-50-1C-54, 179 pp.

DeMaria, M., 1983: Experiments with a spectral tropical cyclone model. Department of Atmospheric Science Paper No. 371, Colorado State University, Ft. Collins, CO, 224 pp.

_____, and W.H. Schubert, 1984: Experiments with a Spectral Tropical Cyclone Model. Journal of the Atmospheric Sciences, v. 41, No. 5, p. 901-924.

Eliasen, E., B. Machenhauer and E. Rasmussen, 1970: On a numerical method for integration of the hydrodynamical equations with spectral representation of the horizontal fields. Report No. 2, Kobenhavens Universitat, Institut for tenetisk meteorolgi.

Emanuel, K.A., 1986: An air-sea interaction theory for tropical cyclones, Part I: Steady state maintenance. Journal of Atmospheric Science, vol. 43, p. 585-604.

Gray, W.M., 1968: Global view of the origin of tropical disturbances and storms. Monthly Weather Review, vol. 96, p. 669-700.

_____, 1970: Hurricanes: their formation, structure and likely role in the tropical circulation. Meteorology Over the Tropical Oceans, D.B. Shaw, ed., Royal Meteorological Society, p. 155-218.

Machenhauer, B., 1979: Numerical methods used in atmospheric models. Vol. II, Chapter 3: The Spectral Method. GARP Publication Series No. 17, p. 121-275.

McBride, J.L., 1979: Observational analysis of tropical cyclone formation. Department of Atmospheric Science Paper No. 308, Colorado State University, Ft. Collins, CO, 230 pp.

_____, and R. Zehr, 1981: Observational analysis of tropical cyclone formation. Part II: Comparison of non-developing versus developing systems. Journal of the Atmospheric Sciences, v. 38, p. 1152-1166.

Merrill, R.T., 1982: A comparison of large and small tropical cyclones. Department of Atmospheric Science Paper No. 352, Colorado State University, Ft. Collins, CO, 75 pp.

_____, 1985: Environmental Influences on Hurricane Intensification, Department of Atmospheric Science Paper No. 394, Colorado State University, Ft. Collins, CO, 156 pp.

Ooyama, K.V., 1964: A dynamical model for the study of tropical cyclone development. Geofis. International., v. 4, p. 187-198.

_____, 1969: Numerical simulation of the life cycle of tropical cyclones. Journal of the Atmospheric Sciences, v. 26, p. 3-40.

_____, 1982: Conceptual evolution of the theory and modeling of the tropical cyclone. Journal of the Meteorological Society of Japan, v. 60, p. 369-379.

Orszag, S.A., 1970: Transform method for the calculation of vector-coupled sums: Application to the spectral form of the vorticity equation. Journal of the Atmospheric Sciences, v. 27, p. 890-895.

Rosenthal, S.L., 1970: A circularly symmetric primitive equation model of tropical cyclone development containing and explicitly water vapor cycle. Monthly Weather Review, v. 98, p. 643-663.

_____, 1971: The response of a tropical cyclone model to variations in boundary layer parameters, initial conditions, lateral boundary conditions, and domain size. Monthly Weather Review, v. 99, p. 767-777.

Rotunno, R., and K.A. Emanuel, 1987: The hurricanse as a finite-amplitude air-sea interaction. 17th Conference on Hurricanse and Tropical Meteorology. American Meteorological Society, p. 321-323.

Schubert, W.H., and M. DeMaria, 1985: Axisymmetric, primitive equation, spectral tropical cyclone model. Part I: Formulation. Journal of the Atmospheric Sciences, v. 42, p. 1213-1224.

Schubert, W.H., and J.J. Hack, 1982: Inertial Stability and tropical cyclone development. Journal of the Atmospheric Sciences, v. 39, p. 1687-1697.

Sundqvist, H., 1970: Numerical simulation of the development of tropical cyclones with a ten-level model. Part II. Tellus, v. 22, p. 504-510.

Weatherford, C.L., 1985: Typhoon Structural Variability. Department of Atmospheric Science Paper No. 391, Colorado State University, Ft. Collins, CO, 77 pp.

Yamasaki, M., 1968: Numerical simulation of tropical cyclone development with the use of primitive equations. Journal of the Meteorological Society of Japan, v. 46, p. 178-201.

END

12-87

DTIC